

# Tidal evolution of hierarchical and inclined systems

A.C.M. Correia · J. Laskar · F. Farago · G. Boué

Received: date / Accepted: date

**Abstract** We investigate the dynamical evolution of hierarchical three-body systems under the effect of tides, when the ratio of the orbital semi-major axes is small and the mutual inclination is relatively large (greater than  $20^\circ$ ). Using the quadrupolar non-restricted approximation for the gravitational interactions and the viscous linear model for tides, we derive the averaged equations of motion in a vectorial formalism which is suitable to model the long-term evolution of a large variety of exoplanetary systems in very eccentric and inclined orbits. In particular, it can be used to derive constraints for stellar spin-orbit misalignment, capture in Cassini states, tidal-Kozai migration, or damping of the mutual inclination. Because our model is valid for the non-restricted problem, it can be used to study systems of identical mass or for the outer restricted problem, such as the evolution of a planet around a binary of stars. Here, we apply our model to three distinct situations: 1) the HD 80606 planetary system, for which we obtain the probability density function distribution for the misalignment angle, with two pronounced peaks of higher probability around  $53^\circ$  and  $109^\circ$ ; 2) the HD 98800 binary system, for which we show that initial prograde orbits inside the observed disc may become retrograde and vice-versa, only because of tidal migration within the binary stars; 3) the HD 11964 planetary system, for which we show that tidal dissipation combined with gravitational perturbations may lead to a decrease in the mutual inclination, and a fast circularization of the inner orbit.

**Keywords** Restricted Problems · Extended Body · Dissipative Forces · Planetary Systems · Rotation

## 1 Introduction

At present, about 50 multi-planet systems have been reported, out of which roughly  $1/3$  possess close-in planets with semi-major axis smaller than 0.1 AU. There are also indications that about half of these stars are likely to have distant companions (Fischer et al, 2001). In addition, close binary star systems (separation smaller than 0.1 AU) are often accompanied by a third star (e.g. D’Angelo et al, 2006). Therefore, although hierarchical systems are considerably different from our Solar system, they represent a significant fraction of the already known systems of stars and planets. These systems are particularly interesting from a dynamical point of view, as they can be stable for very eccentric and inclined orbits and thus present uncommon behaviors. In particular, they become interesting when the two innermost bodies are sufficiently close to undergo significant tidal interactions over the age of the system, since the final outcome of the evolution can be in a configuration that is totally different from the initial one.

The origin and evolution of the orbital configurations of multi-body systems can be analyzed with direct numerical integrations of the full equations of motion, but the understanding of the dynamics often benefits from analytical approximations. Additionally, tidal effects usually act over very long time-scales and therefore approximate theories also allow to speed-up the numerical simulations and to explore the parameter space much more rapidly. Secular perturbation theories based on series expansions have been used for hierarchical triple systems. For low values of the eccentricity, the ex-

pansion of the perturbation in series of the eccentricity is very efficient (e.g. Wu and Goldreich, 2002), but this method is not appropriate for orbits that become very eccentric. An expansion in the ratio of the semi-major axis  $a_1/a_2$  is then preferred, as in this case exact expressions can be computed for the secular system (e.g. Laskar and Boué, 2010).

The development to the second order in  $a_1/a_2$ , called the quadrupole approximation, was used by Lidov (1961, 1962) and Kozai (1962) for the restricted inner problem (the outer orbit is unperturbed). In this case, the conservation of the normal component of the angular momentum enables the inner orbit to periodically exchange its eccentricity with inclination (the so-called Lidov-Kozai mechanism). There is, however, another limit case to the massive problem, which is the outer restricted problem (the inner orbit is unperturbed). Palacián et al (2006) have studied this case and discussed the existence and stability of equilibria in the non-averaged system. Farago and Laskar (2010) derived a simple model of the outer restricted case and described the possible motions of the bodies. They also looked at the quadrupolar problem of three masses and show how the inner and outer restricted cases are related to the general case.

For planar problems, the series expansions in  $a_1/a_2$  should be conducted to the octopole order (e.g. Marchal, 1990; Ford et al, 2000; Laskar and Boué, 2010), as the quadrupole approximation fails to reproduce the eccentricity oscillations (e.g. Lee and Peale, 2003). However, the inclinations of the already known hierarchical systems have not been yet determined, and it can be assumed that high values for the eccentricities may also indicate that their mutual inclinations are large as well (e.g. Laskar, 1997; Chatterjee et al, 2008).

As for Mercury, Venus and the majority of the natural satellites in the Solar system, close-in bodies undergo significant tidal interactions, resulting that their spins and orbits are slowly modified. The ultimate stage for tidal evolution is the synchronization of the spin and the circularization of the orbit. Indeed, the observed mean eccentricity for planets and binary stars with  $a_1 < 0.1$  AU is close to zero within the observational limitations (e.g. Pont et al, 2011). Although tidal effects modify the spin in a much shorter time-scale than they modify the orbit, synchronous rotation can only occur when the eccentricity is very close to zero: the rotation rate tends to be locked with the orbital speed at the periastris, because tidal effects are stronger when the two bodies are closer to each other.

During the formation process, the orbital eccentricity can increase due to gravitational scattering, so that the inner bodies become close enough at periastris for tidal interactions to occur (e.g. Nagasawa et al, 2008).

The same gravitational scattering is simultaneously responsible for an increase of the mutual inclination of the orbits (e.g. Chatterjee et al, 2008), and the fact that inclined systems exchange its inclination with the inner's orbit eccentricity, results that the dissipation in the eccentricity can be transmitted to the inclination of the orbits, and vice-versa. The most striking example is that the spin and the orbit can be completely misaligned (e.g. Pont et al, 2009; Triaud et al, 2010). Previous studies on this subject have been undertaken by Eggleton and Kiseleva-Eggleton (2001) for binary stars and by Wu and Murray (2003) and Fabrycky and Tremaine (2007) for a planet in a wide binary. Despite the success obtained by these works in explaining the observations, they all used the same set of equations, derived by Eggleton and Kiseleva-Eggleton (2001), which is not easy to implement and has been obtained in the frame of the inner restricted quadrupolar approximation. As a consequence, their model cannot be applied to a large number of situations, where the outer orbit cannot be held constant, such as regular planetary systems or planets around close binaries.

In this paper we intend to go deeper into the study of hierarchical three-body systems, where the innermost bodies undergo tidal interactions. We do not make any restrictions on the masses of these bodies, and use the quadrupolar approximation for gravitational interactions with general relativity corrections. Our study is then suitable for binary star systems, planetary systems, and also for planet-satellite systems. We also consider in our model the full effect on the spins of the two closest bodies, including the rotational flattening of their figures. This allows us to correctly describe the precession of the spin axis and subsequent capture in Cassini states. We adopt a viscous linear model for tides (Singer, 1968; Mignard, 1979), as it provides simple expressions for the tidal torques for any eccentricity value. Since we are interested in the secular behavior, we average the motion equations over the mean anomalies of the orbits and express them using the vectorial methods developed by Boué and Laskar (2006), Correia (2009), and Tremaine et al (2009).

In Section 2 we derive the averaged equations of motion that we use to evolve hierarchical systems by tidal effect. In Section 3 we obtain the secular evolution of the spin and orbital quantities in terms of reference angles and elliptical elements, that are useful and more intuitive to understand the outcomes of the numerical simulations. In Section 4 we apply our model to three distinct situations of extra-solar systems: HD 80606, HD 98800, and HD 11964. Finally, last section is devoted to the conclusions.

## 2 The model

We consider here a hierarchical system of bodies composed of a central pair with masses  $m_0$  and  $m_1$ , together with an external companion with mass  $m_2$ . Both inner bodies are considered oblate ellipsoids with gravity field coefficients given by  $J_{2_0}$  and  $J_{2_1}$ , rotating about the axis of maximal inertia along the directions  $\hat{\mathbf{s}}_0$  and  $\hat{\mathbf{s}}_1$  (gyroscopic approximation), with rotation rates  $\omega_0$  and  $\omega_1$ , respectively, such that (e.g. Lambeck, 1988)

$$J_{2_i} = k_{2_i} \frac{\omega_i^2 R_i^3}{3Gm_i}, \quad (1)$$

where  $G$  is the gravitational constant,  $R_i$  is the radius of each body, and  $k_{2_i}$  is the second Love number for potential (pertaining to a perfectly fluid body).

We use Jacobi canonical coordinates, with  $\mathbf{r}_1$  being the position of  $m_1$  relative to  $m_0$ , and  $\mathbf{r}_2$  the position of  $m_2$  relative to the center of mass of  $m_0$  and  $m_1$ . We further assume that  $|\mathbf{r}_1| \ll |\mathbf{r}_2|$ , and we shall refer to the orbit of  $m_1$  relative to  $m_0$  as the inner orbit, and the orbit of  $m_2$  relative to the center of mass of  $m_0$  and  $m_1$  as the outer orbit. In the following, for any vector  $\mathbf{u}$ ,  $\hat{\mathbf{u}} = \mathbf{u}/\|\mathbf{u}\|$  is the unit vector.

### 2.1 Conservative motion

In the quadrupolar three-body problem approximation, the potential energy  $U$  of the system is given by (e.g. Smart, 1953):

$$\begin{aligned} U = & -G \frac{m_0 m_1}{r_1} \left( 1 - \sum_{i=0,1} J_{2_i} \left( \frac{R_i}{r_1} \right)^2 P_2(\hat{\mathbf{r}}_1 \cdot \hat{\mathbf{s}}_i) \right) \\ & -G \frac{m_{01} m_2}{r_2} \left( 1 - \sum_{i=0,1} J_{2_i} \frac{m_i}{m_{01}} \left( \frac{R_i}{r_2} \right)^2 P_2(\hat{\mathbf{r}}_2 \cdot \hat{\mathbf{s}}_i) \right) \\ & -G \frac{\beta_1 m_2}{r_2} \left( \frac{r_1}{r_2} \right)^2 P_2(\hat{\mathbf{r}}_2 \cdot \hat{\mathbf{r}}_1), \end{aligned} \quad (2)$$

where  $P_2(x) = (3x^2 - 1)/2$  is the Legendre polynomial of degree two, and terms in  $(r_1/r_2)^3$  and  $(R_i/r_j)^3$  have been neglected ( $i, j = 0, 1$ ). We also have  $m_{01} = (m_0 + m_1)$ ,  $\beta_1 = m_0 m_1 / m_{01}$ ,  $\beta_2 = m_{01} m_2 / (m_{01} + m_2)$ ,  $\mu_1 = Gm_{01}$ , and  $\mu_2 = G(m_{01} + m_2)$ .

The evolution of the spins can be tracked by the rotational angular momenta,  $\mathbf{L}_i \simeq C_i \omega_i \hat{\mathbf{s}}_i$ . In turn, the evolution of the orbits can be tracked by the orbital angular momenta,  $\mathbf{G}_i = \beta_i \sqrt{\mu_i a_i (1 - e_i^2)} \hat{\mathbf{k}}_i$  (where  $\hat{\mathbf{k}}_i$  is the unit vector  $\hat{\mathbf{G}}_i$ ), and the Laplace-Runge-Lenz vec-

tor, which points along the major axis in the direction of periaxis with magnitude  $e_1$ :

$$\mathbf{e}_1 = \frac{\dot{\mathbf{r}}_1 \times \mathbf{G}_1}{\beta_1 \mu_1} - \frac{\mathbf{r}_1}{r_1}. \quad (3)$$

$a_i$  is the semi-major axis (that can also be expressed using the mean motion,  $n_i = \sqrt{\mu_i/a_i^3}$ ),  $e_i$  is the eccentricity, and  $C_i$  is the principal moment of inertia. The contributions to the orbits are easily computed from the above potentials as

$$\dot{\mathbf{G}}_1 = \mathbf{r}_1 \times \mathbf{F}_1, \quad \dot{\mathbf{G}}_2 = \mathbf{r}_2 \times \mathbf{F}_2, \quad (4)$$

and

$$\dot{\mathbf{e}}_1 = \frac{1}{\beta_1 \mu_1} \left( \mathbf{F}_1 \times \frac{\mathbf{G}_1}{\beta_1} + \dot{\mathbf{r}}_1 \times \dot{\mathbf{G}}_1 \right), \quad (5)$$

where  $\mathbf{F}_i = -\nabla_{\mathbf{r}_i} U'$ , with  $U' = U + Gm_0 m_1 / r_1 + Gm_{01} m_2 / r_2$ .

In Jacobi coordinates, the total orbital angular momentum is equal to  $\mathbf{G}_1 + \mathbf{G}_2$  (e.g. Smart, 1953). Since the total angular momentum is conserved, the contributions to the spin of the bodies can be computed from the orbital contributions:

$$\dot{\mathbf{L}}_0 + \dot{\mathbf{L}}_1 = -(\dot{\mathbf{G}}_1 + \dot{\mathbf{G}}_2). \quad (6)$$

Because we are only interested in the secular evolution of the system, we further average the equations of motion over the mean anomalies of both orbits (see appendix A). The resulting equations are (e.g. Boué and Laskar, 2006; Farago and Laskar, 2010):

$$\begin{aligned} \dot{\mathbf{G}}_1 = & -\gamma(1 - e_1^2) \cos I \hat{\mathbf{k}}_2 \times \hat{\mathbf{k}}_1 + 5\gamma(\mathbf{e}_1 \cdot \hat{\mathbf{k}}_2) \hat{\mathbf{k}}_2 \times \mathbf{e}_1 \\ & - \sum_i \alpha_{1i} \cos \theta_i \hat{\mathbf{s}}_i \times \hat{\mathbf{k}}_1, \end{aligned} \quad (7)$$

$$\begin{aligned} \dot{\mathbf{G}}_2 = & -\gamma(1 - e_1^2) \cos I \hat{\mathbf{k}}_1 \times \hat{\mathbf{k}}_2 + 5\gamma(\mathbf{e}_1 \cdot \hat{\mathbf{k}}_2) \mathbf{e}_1 \times \hat{\mathbf{k}}_2 \\ & - \sum_i \alpha_{2i} \cos \varepsilon_i \hat{\mathbf{s}}_i \times \hat{\mathbf{k}}_2, \end{aligned} \quad (8)$$

$$\begin{aligned} \dot{\mathbf{e}}_1 = & -\frac{\gamma(1 - e_1^2)}{\|\mathbf{G}_1\|} \left[ \cos I \hat{\mathbf{k}}_2 \times \mathbf{e}_1 - 2\hat{\mathbf{k}}_1 \times \mathbf{e}_1 - 5(\mathbf{e}_1 \cdot \hat{\mathbf{k}}_2) \hat{\mathbf{k}}_2 \times \hat{\mathbf{k}}_1 \right] \\ & - \sum_i \frac{\alpha_{1i}}{\|\mathbf{G}_1\|} \left[ \cos \theta_i \hat{\mathbf{s}}_i \times \mathbf{e}_1 + \frac{1}{2}(1 - 5 \cos^2 \theta_i) \hat{\mathbf{k}}_1 \times \mathbf{e}_1 \right], \end{aligned} \quad (9)$$

and

$$\dot{\mathbf{L}}_i = -\alpha_{1i} \cos \theta_i \hat{\mathbf{k}}_1 \times \hat{\mathbf{s}}_i - \alpha_{2i} \cos \varepsilon_i \hat{\mathbf{k}}_2 \times \hat{\mathbf{s}}_i, \quad (10)$$

where

$$\alpha_{1i} = \frac{3Gm_0 m_1 J_{2_i} R_i^2}{2a_1^3 (1 - e_1^2)^{3/2}}, \quad (11)$$

$$\alpha_{2i} = \frac{3Gm_2 m_i J_{2_i} R_i^2}{2a_2^3 (1 - e_2^2)^{3/2}}, \quad (12)$$

$$\gamma = \frac{3Gm_2\beta_1 a_1^2}{4a_2^3(1-e_2^2)^{3/2}}, \quad (13)$$

and

$$\cos \theta_i = \hat{\mathbf{s}}_i \cdot \hat{\mathbf{k}}_1, \quad \cos \varepsilon_i = \hat{\mathbf{s}}_i \cdot \hat{\mathbf{k}}_2, \quad \cos I = \hat{\mathbf{k}}_1 \cdot \hat{\mathbf{k}}_2, \quad (14)$$

are the direction cosines of the spins and orbits:  $\theta_i$  is the obliquity to the orbital plane of the inner orbit,  $\varepsilon_i$  is the obliquity to the orbital plane of the outer companion, and  $I$  is the inclination between orbital planes. They can also be expressed as

$$\cos \varepsilon_i = \cos I \cos \theta_i + \sin I \sin \theta_i \cos \varphi_i, \quad (15)$$

where  $\varphi_i$  is a precession angle.

## 2.2 General relativity correction

We may add to Newton's equations the dominant contribution from general relativistic effects. These effects are mainly felt by eccentric orbits on close encounters between the central bodies and contribute to the gravitational force with a small correction (e.g. Schutz, 1985)

$$\mathbf{F}_{\text{gr}} = -\frac{3\mu_1 \|\mathbf{G}_1\|^2}{\beta_1 c^2 r_1^4} \hat{\mathbf{r}}_1, \quad (16)$$

where  $\|\mathbf{G}_1\| = \beta_1 \sqrt{\mu_1 a_1 (1 - e_1^2)}$ , and  $c$  is the speed of light. To this order, the dominant relativistic secular contribution is on the precession of the periastris, leaving eccentricity, orientation and semi-major axis of the orbit unaffected (Eq. 5):

$$\dot{\mathbf{e}}_1 = \frac{3\mu_1 n_1}{c^2 a_1 (1 - e_1^2)} \hat{\mathbf{k}}_1 \times \mathbf{e}_1. \quad (17)$$

## 2.3 Tidal effects

Neglecting the tidal interactions with the external body  $m_2$ , the tidal potential for the inner pair writes (e.g. Kaula, 1964):

$$U_T = -\frac{G}{r_1^3} \sum_{i=0,1} k_{2i} m_{(1-i)}^2 \frac{R_i^5}{r_1^3} P_2(\hat{\mathbf{r}}_1 \cdot \hat{\mathbf{r}}'_1), \quad (18)$$

where  $\mathbf{r}'_1$  is the position of the interacting body at a time delayed of  $\Delta t_i$ . The dissipation of the mechanical energy of tides in the body's interior is responsible for this delay between the initial perturbation and the maximal deformation. As the rheology of stars and planets is badly known, the exact dependence of  $\Delta t_i$  on the tidal frequency is unknown. Many different authors have studied the problem and several models have been developed so far, from the simplest ones to the more complex (for a review see Correia et al, 2003; Efroimsky and Williams, 2009). The huge problem in validating one model better than others is the difficulty to

compare the theoretical results with the observations, as the effect of tides are very small and can only be detected efficiently after long periods of time. The qualitative conclusions are more or less unaffected, so, for simplicity, we adopt here a model with constant  $\Delta t_i$ , which can be made linear (Mignard, 1979; Néron de Surgy and Laskar, 1997):

$$\mathbf{r}'_1 \simeq \mathbf{r}_1 + \Delta t_i (\omega_i \hat{\mathbf{s}}_i \times \mathbf{r}_1 - \dot{\mathbf{r}}_1). \quad (19)$$

As for the conservative motion, we can obtain the equations of motion directly from equations (4), (5) and (6) using  $U_T$  instead of  $U'$  (see appendix A), that is,

$$\dot{\mathbf{G}}_2 = 0, \quad \dot{\mathbf{G}}_1 = -\dot{\mathbf{L}}_0 - \dot{\mathbf{L}}_1, \quad (20)$$

$$\begin{aligned} \dot{\mathbf{e}}_1 = & \sum_i \frac{15}{2} k_{2i} n_1 \left( \frac{m_{(1-i)}}{m_i} \right) \left( \frac{R_i}{a_1} \right)^5 f_4(e_1) \hat{\mathbf{k}}_1 \times \mathbf{e}_1 \\ & - \sum_i \frac{K_i}{\beta_1 a_1^2} \left[ f_4(e_1) \frac{\omega_i}{2n_1} (\mathbf{e}_1 \cdot \hat{\mathbf{s}}_i) \hat{\mathbf{k}}_1 \right. \\ & \left. - \left( \frac{11}{2} f_4(e_1) \cos \theta_i \frac{\omega_i}{n_1} - 9f_5(e_1) \right) \mathbf{e}_1 \right], \end{aligned} \quad (21)$$

and

$$\begin{aligned} \dot{\mathbf{L}}_i = & K_i n_1 \left[ f_4(e_1) \sqrt{1 - e_1^2} \frac{\omega_i}{2n_1} (\hat{\mathbf{s}}_i - \cos \theta_i \hat{\mathbf{k}}_1) \right. \\ & \left. - f_1(e_1) \frac{\omega_i}{n_1} \hat{\mathbf{s}}_i + f_2(e_1) \hat{\mathbf{k}}_1 + \frac{(\mathbf{e}_1 \cdot \hat{\mathbf{s}}_i)(6 + e_1^2)}{4(1 - e_1^2)^{9/2}} \frac{\omega_i}{n_1} \mathbf{e}_1 \right], \end{aligned} \quad (22)$$

where,

$$K_i = \Delta t_i \frac{3k_{2i} G m_{(1-i)}^2 R_i^5}{a_1^6}, \quad (23)$$

and

$$f_1(e) = \frac{1 + 3e^2 + 3e^4/8}{(1 - e^2)^{9/2}}, \quad (24)$$

$$f_2(e) = \frac{1 + 15e^2/2 + 45e^4/8 + 5e^6/16}{(1 - e^2)^6}, \quad (25)$$

$$f_3(e) = \frac{1 + 31e^2/2 + 255e^4/8 + 185e^6/16 + 25e^8/64}{(1 - e^2)^{15/2}}, \quad (26)$$

$$f_4(e) = \frac{1 + 3e^2/2 + e^4/8}{(1 - e^2)^5}, \quad (27)$$

$$f_5(e) = \frac{1 + 15e^2/4 + 15e^4/8 + 5e^6/64}{(1 - e^2)^{13/2}}. \quad (28)$$

The first term in expression (21) corresponds to a permanent tidal deformation, while the second term corresponds to the dissipative contribution. The precession rate of  $\mathbf{e}_1$  about  $\hat{\mathbf{k}}_1$  is usually much faster than the evolution time-scale for the dissipative tidal effects. As a consequence, when the eccentricity is constant over a precession cycle, we can average expression (23) over

the argument of the periapsis and get (Correia, 2009, appendix A):

$$\dot{\mathbf{L}}_i = -K_i n_1 \left( f_1(e_1) \frac{\hat{\mathbf{s}}_i + \cos \theta_i \hat{\mathbf{k}}_1}{2} \frac{\omega_i}{n_1} - f_2(e_1) \hat{\mathbf{k}}_1 \right) \quad (29)$$

### 3 Secular evolution

We have presented the equations that rule the tidal evolution of a hierarchical system of three bodies in terms of a vectorial formalism. However, the spin and orbital quantities are better represented by the rotation angles and elliptical elements. The direction cosines (Eq. 14) are obtained from the angular momenta vectors, since  $\hat{\mathbf{s}}_i = \mathbf{L}_i / \|\mathbf{L}_i\|$  and  $\hat{\mathbf{k}}_i = \mathbf{G}_i / \|\mathbf{G}_i\|$ , as well as the rotation rate  $\omega_i = \mathbf{L}_i \cdot \hat{\mathbf{s}}_i / C_i$ . The eccentricity and the semi-major axis can be obtained from  $e_1 = \|\mathbf{e}_1\|$  and  $a_1 = \|\mathbf{G}_1\|^2 / (\beta_1^2 \mu_1 (1 - e_1^2))$ , respectively.

#### 3.1 Conservative motion

##### 3.1.1 Cassini states

The obliquities are functions of  $\mathbf{G}_1$ ,  $\mathbf{G}_2$ , and  $\mathbf{L}_i$  (Eq. 14). Their evolution can be obtained from (Eqs. 7, 8, 10) as

$$\frac{d \cos \theta_i}{dt} = \frac{\dot{\mathbf{G}}_1 \cdot (\hat{\mathbf{s}}_i - \cos \theta_i \hat{\mathbf{k}}_1)}{\|\mathbf{G}_1\|} + \frac{\dot{\mathbf{L}}_i \cdot (\hat{\mathbf{k}}_1 - \cos \theta_i \hat{\mathbf{s}}_i)}{\|\mathbf{L}_i\|}, \quad (30)$$

for the obliquity to the orbital plane of the inner orbit,  $\theta_i$ . An identical expression could be obtained for the obliquity to the outer orbit,  $\varepsilon_i$ , replacing  $\mathbf{G}_1$  by  $\mathbf{G}_2$ . To simplify, we may average the equations over the argument of the periapsis (appendix A), and the norms of  $\|\mathbf{G}_1\|$ ,  $\|\mathbf{G}_2\|$ , and  $\|\mathbf{L}_i\|$  become constant. Thus,

$$\frac{d \cos \theta_i}{dt} = \frac{d \hat{\mathbf{k}}_1}{dt} \cdot (\hat{\mathbf{s}}_i - \cos \theta_i \hat{\mathbf{k}}_1) + \frac{d \hat{\mathbf{s}}_i}{dt} \cdot (\hat{\mathbf{k}}_1 - \cos \theta_i \hat{\mathbf{s}}_i), \quad (31)$$

where

$$\begin{aligned} \frac{d \hat{\mathbf{k}}_1}{dt} &= -\frac{\gamma}{\|\mathbf{G}_1\|} \left( 1 + \frac{3}{2} e_1^2 \right) \cos I \hat{\mathbf{k}}_2 \times \hat{\mathbf{k}}_1 \\ &\quad - \sum_i \frac{\alpha_{1i}}{\|\mathbf{G}_1\|} \cos \theta_i \hat{\mathbf{s}}_i \times \hat{\mathbf{k}}_1, \end{aligned} \quad (32)$$

and

$$\frac{d \hat{\mathbf{s}}_i}{dt} = -\frac{\alpha_{1i}}{\|\mathbf{L}_i\|} \cos \theta_i \hat{\mathbf{k}}_1 \times \hat{\mathbf{s}}_i - \frac{\alpha_{2i}}{\|\mathbf{L}_i\|} \cos \varepsilon_i \hat{\mathbf{k}}_2 \times \hat{\mathbf{s}}_i. \quad (33)$$

This system has *a priori* four degrees of freedom associated to the four precession angles (one for each orbit, and one per solid body). However, because the total angular momentum is conserved, there is only three degrees of freedom. Regular solutions of (Eqs. 31, 33, 33)

are thus combination of three eigenmodes. More precisely, these solutions are composed of a uniform rotation of all the vectors around the total angular momentum, and in the rotating frame, vectors describe quasi-periodic motions with only 2 proper frequencies (Boué and Laskar, 2006, 2009). The bodies are in an equilibrium configuration, usually called *Cassini state*, when the amplitudes of the quasi-periodic motion vanish. Although analytical approximations of the solutions can be obtained (Boué and Laskar, 2006, 2009), we assume that  $\alpha_{2i} \ll \alpha_{1i} \ll \gamma$ , and also  $\|\mathbf{G}_1\| \ll \|\mathbf{G}_2\|$ . Then, equation (33) simplifies

$$\frac{d \hat{\mathbf{k}}_1}{dt} \approx -\frac{\gamma}{\|\mathbf{G}_1\|} \left( 1 + \frac{3}{2} e_1^2 \right) \cos I \hat{\mathbf{k}}_2 \times \hat{\mathbf{k}}_1. \quad (34)$$

The evolution of  $\mathbf{G}_1$  is thus independent of  $\mathbf{L}_i$ , and it has a uniform precession motion at frequency  $g$  around the total orbital angular momentum, where

$$g \approx -\frac{\gamma}{\|\mathbf{G}_1\|} \left( 1 + \frac{3}{2} e_1^2 \right) \cos I. \quad (35)$$

The evolution of the spin-axes is then simpler in the rotating frame where  $\hat{\mathbf{k}}_1$  and  $\hat{\mathbf{k}}_2$  are constant. Since  $\alpha_{1i} \gg \alpha_{2i}$ , we have for each body

$$\frac{d \hat{\mathbf{s}}_i}{dt} = -\frac{\alpha_{1i}}{\|\mathbf{L}_i\|} \cos \theta_i \hat{\mathbf{k}}_1 \times \hat{\mathbf{s}}_i - g \hat{\mathbf{k}}_2 \times \hat{\mathbf{s}}_i, \quad (36)$$

which leads to

$$\dot{\theta}_i = g \sin I \sin \varphi_i, \quad (37)$$

and

$$\dot{\varphi}_i = -\left( \frac{\alpha_{1i}}{\|\mathbf{L}_i\|} \cos \theta_i + g \cos I \right) + g \sin I \frac{\cos \varphi_i}{\tan \theta_i}. \quad (38)$$

We used the fact that  $\hat{\mathbf{k}}_1$  and  $\hat{\mathbf{k}}_2$  are coplanar. Equation (37) shows that the obliquity is oscillating around an equilibrium value given by  $\varphi_i = 0$  or  $\pi$ . Stable configurations for the spin can be found whenever the vectors  $(\hat{\mathbf{s}}_i, \hat{\mathbf{k}}_1, \hat{\mathbf{k}}_2)$  are coplanar and precess at the same rate  $g$  (e.g. Colombo, 1966; Peale, 1969). The equilibrium obliquities can be found setting  $\dot{\varphi}_i = 0$  (Eq. 38), which provides a single relationship (e.g. Ward and Hamilton, 2004):

$$\lambda_i \cos \theta_i \sin \theta_i + \sin(\theta_i - I) = 0, \quad (39)$$

where  $\lambda_i = \alpha_{1i} / (\|\mathbf{L}_i\| g)$  is a dimensionless parameter. The above equation has two or four real roots for  $\theta_i$ , which are known by *Cassini states*. For nearly coplanar orbits, we have  $I \sim 0$ , and these solutions are approximately given by:

$$\tan^{-1} \left( \frac{\sin I}{\cos I \pm \lambda_i} \right), \quad \pm \cos^{-1} \left( -\frac{\cos I}{\lambda_i} \right). \quad (40)$$

For a generic value of  $I$ , when  $|\lambda_i| \ll 1$  the first expression gives the only two real roots of equation (39). On the other hand, when  $|\lambda_i| \gg 1$ , we have four real roots approximately given by expressions (40).

### 3.1.2 Lidov-Kozai cycles

The variations in the mutual inclination between the inner orbit and the orbit of the external companion can be obtained from the direction cosine (Eq.14) in a similar way as the obliquity (Eq.30):

$$\frac{d \cos I}{dt} = \frac{\dot{\mathbf{G}}_1 \cdot (\hat{\mathbf{k}}_2 - \cos I \hat{\mathbf{k}}_1)}{\|\mathbf{G}_1\|} + \frac{\dot{\mathbf{G}}_2 \cdot (\hat{\mathbf{k}}_1 - \cos I \hat{\mathbf{k}}_2)}{\|\mathbf{G}_2\|}. \quad (41)$$

Since  $\|\mathbf{G}_1\| \ll \|\mathbf{G}_2\|$ , we obtain from expression (7):

$$\begin{aligned} \frac{d \cos I}{dt} &= \frac{5}{2} \frac{\gamma e_1^2}{\|\mathbf{G}_1\|} \cos I \sin^2 I \sin 2\varpi_1 \\ &\quad - \sum_i \frac{\alpha_{1i} \cos \theta_i}{\|\mathbf{G}_1\|} (\hat{\mathbf{s}}_i \times \hat{\mathbf{k}}_1) \cdot \hat{\mathbf{k}}_2, \end{aligned} \quad (42)$$

where  $\varpi_1$  is the argument of the periapsis of the inner orbit, that is, the angle between the line of nodes of the two orbits and the periapsis of the inner orbit.

On the other hand, the variations in the eccentricity are easily obtained from the Laplace-Runge-Lenz vector (Eq.9):

$$\dot{e}_1 = \frac{\dot{\mathbf{e}}_1 \cdot \mathbf{e}_1}{e_1} = \frac{5}{2} \frac{\gamma (1 - e_1^2) e_1}{\|\mathbf{G}_1\|} \sin^2 I \sin 2\varpi_1. \quad (43)$$

Thus, combining expressions (43) and (43) and neglecting the contributions from the rotational flattening (terms in  $\alpha_{1i}$ ), we get

$$\frac{d \cos I}{dt} = \frac{e_1 \dot{e}_1}{(1 - e_1^2)} \cos I, \quad (44)$$

which can be integrated to give

$$\sqrt{1 - e_1^2} \cos I = h_1 = Cte, \quad (45)$$

where  $h_1$  is constant in absence of tides. The above relation shows that an increase in the eccentricity of the inner orbit must be accompanied by a decrease in the mutual inclination and vice-versa. It corresponds to a *happy coincidence*, as called by Lidov and Ziglin (1976), which results from the fact that in the quadrupolar approximation the potential energy (Eq.2) does not depend on argument of the periapsis of the external body  $\varpi_2$  (e.g. Farago and Laskar, 2010). As a consequence, the conjugate Delaunay variable  $\|\mathbf{G}_2\| = \beta_2 \sqrt{\mu_2 a_2 (1 - e_2^2)}$  is constant, and, as the semi-major axis are constant in the secular problem,  $e_2$  is also constant. Indeed, when we consider only the orbital contributions, the total angular momentum is

$$\|\mathbf{G}_1\|^2 + \|\mathbf{G}_2\|^2 + 2 \|\mathbf{G}_1\| \|\mathbf{G}_2\| \cos I = Cte. \quad (46)$$

Since  $\|\mathbf{G}_2\|$  is constant and  $\|\mathbf{G}_1\| \ll \|\mathbf{G}_2\|$ , it remains  $\|\mathbf{G}_1\| \cos I = Cte$ , and we retrieve the result given by equation (45). This is no longer true for the octopole or higher order approximations (e.g. Laskar and Boué, 2010).

The variations in the inclination and eccentricity (Eqs. 43, 43) become zero when  $\sin 2\varpi_1 = 0$ , that is, for  $\cos 2\varpi_1 = \pm 1$ . When  $\cos 2\varpi_1 = -1$  ( $\varpi_1 = \pm \pi/2$ ) it is possible to show that  $\dot{\varpi} = 0$  has a solution if  $h_1 \leq \sqrt{3/5}$  (Lidov, 1962; Kozai, 1962). Thus, when the mutual inclination is greater than  $\arccos \sqrt{3/5} \simeq 39.23^\circ$  we have a libration regime for the periapsis about  $\varpi_1 = \pm \pi/2$ . In this regime, one can observe large variations in both  $I$  and  $e_1$ , known by *Lidov-Kozai cycles*. If the inner orbit is initially circular, the maximum eccentricity achieved is given by  $e_1 = \sqrt{1 - (5/3) \cos^2 I}$ .

Lidov-Kozai cycles persist as long as the perturbation from the outer body is the dominant cause of precession in the inner orbit. However, additional sources of precession, such as general relativity or tides, can compensate the libration mechanism and suppress the large eccentricity/inclination oscillations (e.g. Migaszewski and Goździewski, 2009). For  $h_1 > \sqrt{3/5}$  the periapsis of the inner orbit is always in a circularization regime, so there is only small variations in the eccentricity and inclination.

## 3.2 Tidal evolution

### 3.2.1 Spin evolution

The variation in the body's rotation rate can be computed from equation (29) as  $\dot{\omega}_i = \dot{\mathbf{L}}_i \cdot \hat{\mathbf{s}}_i / C_i$ , giving (Correia and Laskar, 2010a):

$$\dot{\omega}_i = -\frac{K_i n_1}{C_i} \left( f_1(e_1) \frac{1 + \cos^2 \theta_i}{2} \frac{\omega_i}{n_1} - f_2(e_1) \cos \theta_i \right). \quad (47)$$

For a given obliquity and eccentricity, the equilibrium rotation rate, obtained when  $\dot{\omega}_i = 0$ , is attained for:

$$\frac{\omega_i}{n_1} = \frac{f_2(e_1)}{f_1(e_1)} \frac{2 \cos \theta_i}{1 + \cos^2 \theta_i}, \quad (48)$$

Notice, however, that the above expression is only valid for constant eccentricity (and also constant semi-major axis), or at least if tidal effects modify the eccentricity faster than other effects. Indeed, when the eccentricity is forced by the gravitational perturbations from a companion body, the limit solution of expression (47) is no longer given by equation (48), but more generally (Correia and Laskar, 2004, 2009):

$$\frac{\omega_i(t)}{n_1} = \frac{K_i}{C_i g_i(t)} \int_0^t f_2(e_1(\tau)) \cos \theta_i(\tau) g_i(\tau) d\tau, \quad (49)$$

with

$$g_i(t) = \exp \left( \frac{K_i}{2C_i} \int_0^t f_1(e_1(\tau)) (1 + \cos^2 \theta_i(\tau)) d\tau \right). \quad (50)$$

It corresponds to a solution that pursues the instantaneous equilibrium rotation for a given eccentricity (Eq.48), but delayed and with a smaller amplitude, depending on the relative strength of tidal effects. The stronger these effects are, the shorter is the time delay and closer are the amplitudes to expression (48).

In turn, the dissipative obliquity variations are computed by substituting equation (29) in (30) with  $\|\mathbf{L}_i\| \ll \|\mathbf{G}_1\|$ , giving:

$$\dot{\theta}_i \simeq \frac{K_i n_1}{C_i \omega_i} \sin \theta_i \left( f_1(e_1) \cos \theta_i \frac{\omega_i}{2n_1} - f_2(e_1) \right). \quad (51)$$

Because of the factor  $n_1/\omega_i$  in the magnitude of the obliquity variations, for an initial fast rotating body, the time-scale for the obliquity evolution is longer than the time-scale for the rotation rate evolution (Eq.47). As a consequence, it is expected that the rotation rate approaches its equilibrium value (Eq.48) earlier than the obliquity. Replacing equation (48) in (51), we have for constant eccentricity:

$$\dot{\theta}_i \simeq -\frac{K_i n_1}{C_i \omega_i} f_2(e_1) \frac{\sin \theta_i}{1 + \cos^2 \theta_i}. \quad (52)$$

We then conclude that, although the initial behavior of the obliquity depends on the initial rotation rate, tidal effects always end by decreasing the obliquity, since  $\dot{\theta}_i \leq 0$ . Thus, the final obliquity tends to be captured in a small obliquity Cassini state (Eq.40), that is,

$$\theta_i \simeq -\frac{\sin I}{\lambda_i} = \frac{C_i \omega_i \gamma}{\alpha_{1i} \|\mathbf{G}_1\|} \left( 1 + \frac{3}{2} e_1^2 \right) \cos I \sin I. \quad (53)$$

### 3.3 Orbital evolution

The variations in the norm of the orbital angular momentum can be computed directly from expression (29), since  $\dot{\mathbf{G}}_1 = -\dot{\mathbf{L}}_0 - \dot{\mathbf{L}}_1$ :

$$\begin{aligned} \frac{d}{dt} \|\mathbf{G}_1\| &= -\sum_i \dot{\mathbf{L}}_i \cdot \mathbf{k}_1 \\ &= \sum_i K_i n_1 \left( f_1(e_1) \cos \theta_i \frac{\omega_i}{n_1} - f_2(e_1) \right). \end{aligned} \quad (54)$$

The variations in the eccentricity are easily obtained from the Laplace-Runge-Lenz vector (Eq.21):

$$\begin{aligned} \dot{e}_1 &= \frac{\dot{\mathbf{e}}_1 \cdot \mathbf{e}_1}{e_1} \\ &= \sum_i \frac{9K_i}{\beta_1 a_1^2} \left( \frac{11}{18} f_4(e_1) \cos \theta_i \frac{\omega_i}{n_1} - f_5(e_1) \right) e_1, \end{aligned} \quad (55)$$

while the semi-major axis variations are obtained from the eccentricity and the norm of the orbital angular momentum:

$$\frac{\dot{a}_1}{a_1} = \frac{2\dot{e}_1 e_1}{(1 - e_1^2)} + \frac{2\dot{\mathbf{G}}_1 \cdot \mathbf{G}_1}{\|\mathbf{G}_1\|^2}$$

$$= \sum_i \frac{2K_i}{\beta_1 a_1^2} \left( f_2(e_1) \cos \theta_i \frac{\omega_i}{n_1} - f_3(e_1) \right). \quad (56)$$

The inner orbit can either expand or contract, depending on the initial spin of the bodies. Considering for simplicity dissipation in only one component, for fast initial rotating rates ( $\omega_i \gg n_1$ ), the semi-major axis and the eccentricity usually increase, except for retrograde spins ( $\theta_i > \pi/2$ ). The ratio between orbital and spin evolution time-scales is roughly given by  $C_i/(m_1 a_1^2) \ll 1$ , meaning that the spin achieves an equilibrium position much faster than the orbit. Thus, as the rotation rate decreases, the increasing tendency in the orbital parameters is reversed when  $d\|\mathbf{G}_1\|/dt = 0$  (Eq. 54),

$$\frac{\omega_i}{n_1} \cos \theta_i = \frac{f_2(e_1)}{f_1(e_1)}, \quad (57)$$

that is, when the rotation rate is close to its equilibrium value (Eq. 48). After an initial increase in the semi-major axis and in the eccentricity, we can then always expect a contraction of the inner orbit until it becomes completely circularized. The final evolution of the system is then achieved when  $e_1 = 0$ ,  $\omega_i = n_1$  (Eq.48) and  $\theta_i \simeq -\sin I/\lambda_i$  (Eq.53).

The variations in the mutual inclination can be obtained using expression (41) with  $\dot{\mathbf{G}}_1 = -\sum_i \dot{\mathbf{L}}_i$  (Eq. 29). We have then:

$$\frac{d \cos I}{dt} = \sum_i \frac{K_i \omega_i}{2 \|\mathbf{G}_1\|} f_1(e_1) (\cos \varepsilon_i - \cos I \cos \theta_i), \quad (58)$$

or, making use of expression (15),

$$\frac{dI}{dt} = -\sum_i \frac{K_i \omega_i}{2 \|\mathbf{G}_1\|} f_1(e_1) \sin \theta_i \cos \varphi_i. \quad (59)$$

Just after the spin of one body is trapped in a small obliquity Cassini state,  $\varphi_i = 0$  and  $\sin \theta_i$  is constant and given by expression (53). Thus,

$$\frac{dI}{dt} \simeq \sum_i \frac{K_i \omega_i}{2 \lambda_i \|\mathbf{G}_1\|} f_1(e_1) \sin I. \quad (60)$$

## 4 Application to exoplanets

In this section we apply the model described in Sect. 2 to three distinct situations of exoplanetary systems: HD 80606 (inner restricted problem), HD 98800 (outer restricted problem), and HD 11964 (intermediate non-restricted problem). We numerically integrate the set of equations (7), (8), (9), (10) and (17) for the conservative motion, together with equations (20), (21) and (23) for tidal effects.

There exist many systems containing a “hot Jupiter” in a wide binary for which one could apply the present

model to illustrate the tidal migration combined with Lidov-Kozai cycles. However, we prefer to reproduce the results for HD 80606 in order to compare our results (obtained with a non-restricted model) with previous studies by Wu and Murray (2003) and Fabrycky and Tremaine (2007) (obtained with a restricted model).

The stability of a disc around the multi-binary HD 98800 system has been recently studied by Verrier and Evans (2009) and Farago and Laskar (2010), which have isolated two different regimes for the trajectories of the disc. We then apply our model to an hypothetical planet around the binary stars and show how transitions between the two regimes are possible, and how particles in initial prograde orbits may end in retrograde orbits.

We finally use our model to study the HD 11964 system, which is a hierarchical planetary system composed of two planets, the inner one in the Neptune-mass regime and the outer one similar to Jupiter. There is no determination of the mutual inclination between the two planets, but the system is stable for very large values, so we analyze its behavior for different situations.

#### 4.1 HD 80606

In current theories of planetary formation, the region within 0.1 AU of a protostar is too hot and rarefied for a Jupiter-mass planet to form, so “hot Jupiters” likely form further away and then migrate inward. A significant fraction of “hot Jupiters” has been found in systems of binary stars (e.g. Eggenberger et al, 2004), suggesting that the stellar companion may play an important role in the shrinkage of the planetary orbits. In addition, close binary stars (separation comparable to the stellar radius) are also often accompanied by a third star. For instance, Tokovinin et al (2006) found that 96% of a sample of spectroscopic binaries with periods less than 3 days has a tertiary component. Indeed, in some circumstances the distant companion induces tidal interactions in the inner binary by means of the Lidov-Kozai mechanism (Sect. 3.1.2), causing the binary semi-major axis to shrink to the currently observed values (e.g. Eggleton and Kiseleva-Eggleton, 2001). The same mechanism has been subsequently proposed to be at the origin of “hot Jupiters” as an alternative to migration in a disk (e.g. Wu and Murray, 2003).

The HD 80606 system is composed of two Sun-like stars in a very wide orbit ( $a_2 \sim 1000$  AU) (Eggenberger et al, 2004), and a short-period planet in a very eccentric orbit ( $a_1 = 0.45$  AU and  $e_1 = 0.92$ ) (Naef et al, 2001). Because at periapsis the distance to the main star is only 0.036 AU, the orbit of the planet is still un-

**Table 1** Initial parameters for the HD 80606 system (Naef et al, 2001; Eggenberger et al, 2004; Wu and Murray, 2003).

HD 80606			
parameter	body 0	body 1	body 2
$m$ ( $M_\odot$ )	1.1	0.0037	1.1
$P_{\text{rot}}$ (day)	20	0.5	—
$\theta$ (deg)	10	35	—
$\varphi$ (deg)	0	0	—
$R$ ( $\times 10^6$ m)	695	75	—
$C/mR^2$	0.08	0.25	—
$k_2$	0.028	0.51	—
$\Delta t$ (s)	0.1	40	—
parameter	orbit 1		orbit 2
$a$ (AU)	5.0		1000
$e$	0.1		0.5
$\varpi$ (deg)	0.0		—
$I$ (deg)	85.6		

dergoing tidal evolution, and is thus a perfect example to test our model.

In order to compare our results with the previous studies of Wu and Murray (2003) and Fabrycky and Tremaine (2007) we use the same initial conditions for the planet and the stellar companions: the planet is initially set in a Jupiter-like orbit with  $a_1 = 5$  AU,  $e_1 = 0.1$ , and  $I = 85.6^\circ$ , while the stellar companion is supposed to be a Sun-like star at  $a_2 = 1000$  AU, and  $e_2 = 0.5$  (Table 1). In Figure 1 we plot an example of combined tidal-Kozai migration of the planet HD 80606 b.

Prominent eccentricity oscillations are seen from the very beginning and the energy in the planet’s spin is transferred to the orbit increasing the semi-major axis for the first 0.1 Gyr (Eq. 47). As the equilibrium rotation is approached around 0.3 Gyr (Eq. 49) the tidal evolution is essentially controlled by equations (55) and (56), whose contributions are enhanced when the eccentricity reaches high values. The semi-major axis evolution is executed by apparent “discontinuous” transitions precisely because the tidal dissipation is only efficient during periods of high eccentricity. As dissipation reduces the semi-major axis, periapsis precession becomes gradually dominated by general relativity rather than by the third body, and the periapsis starts circulating as the eccentricity approaches to 0 near 0.5 Gyr. Tidal evolution stops when the orbit is completely circularized. The final semi-major axis is estimated to about  $a_f = a_1(1 - e_1^2) \simeq 0.07$  AU, which corresponds to a regular “hot Jupiter” (Correia and Laskar, 2010b).

The angle between the spin axis of the planet and its orbit (denoted by  $\theta_1$ ) is quickly brought by tides to a small obliquity Cassini state (Eq. 53). On the other hand, the angle between the spin axis of the star and the orbit of the planet (denoted by  $\theta_0$ ) is not tidally evolved,



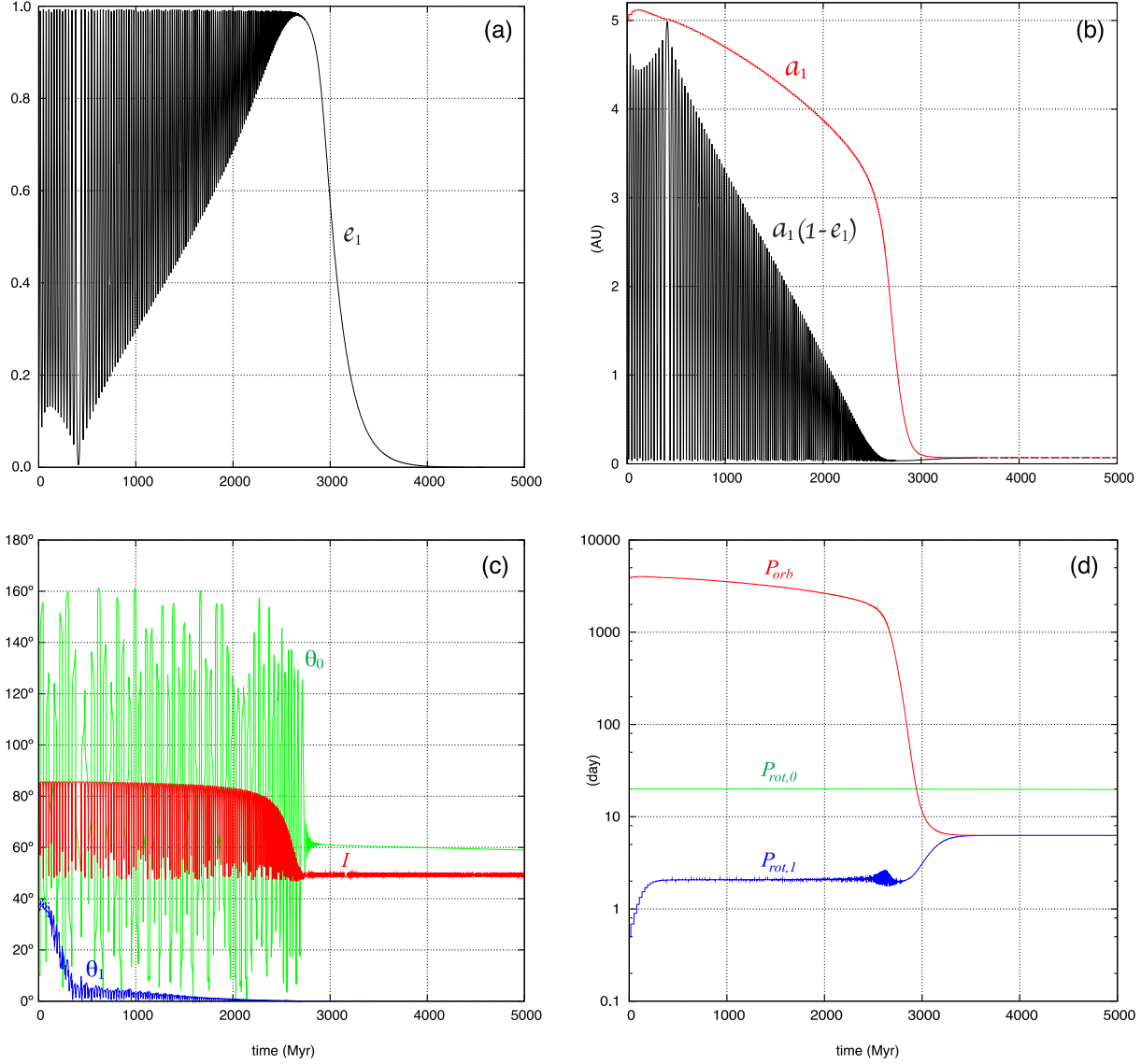


**Fig. 1** Possible evolution of the planet HD 80606 b initially in an orbit with  $a_1 = 5$  AU,  $e_1 = 0.1$ , and  $I = 85.6^\circ$  (Table 1). We show the evolution of the eccentricity  $e_1$  (a), semi-major axis  $a_1$ , and periastris  $a_1(1 - e_1)$  (b), mutual inclination  $I$ , obliquity of the star  $\theta_0$ , and obliquity of the planet  $\theta_1$  (c), and orbital period  $P_{orb}$ , rotation period of the star  $P_{rot,0}$ , and rotation period of the planet  $P_{rot,1}$  (d). Results plot here are identical to those in Wu and Murray (2003) and Fabrycky and Tremaine (2007), obtained with a restricted model.

since the dissipation within the star is much smaller than the dissipation within the planet ( $k_{20} \Delta t_0 \ll k_{21} \Delta t_1$ , Table 1). As a consequence, capture of the spin of the star in a Cassini state does not occur during the time length of the simulations, but one can observe large oscillations corresponding to the variations in the orientation of the orbital plane of the planet. Indeed, as long as  $\alpha_{10} \ll \gamma$ , the angle between the spin of the star and the outer companion (denoted by  $\varepsilon_0$ ) is approximately constant (Eq. 36), and thus  $|\varepsilon_0 - I| \leq \theta_0 \leq \varepsilon_0 + I$  (Eq. 15). In our simulation  $\varepsilon_0 = 85.6^\circ - 10^\circ = 75.6^\circ$  (Table 1), so we approximately observe that  $10^\circ \leq \theta_0 \leq 161^\circ$  (Figure 1c).

As the semi-major axis decreases, the precession of the planet's orbit becomes progressively dominated by the equatorial bulge of the star, so that  $\alpha_{10} \sim \gamma$  around 2.8 Gyr (Eq. 33). From that point, the orbit of the planet precesses around the spin of the star and  $\theta_0$  becomes constant, retaining a value between  $10^\circ$  and  $160^\circ$ . One then expects to observe a misalignment between the spin of the star and the orbit of the planet. In the simulation shown in Figure 1, we obtain  $\theta_0 \approx 60^\circ$ , but this value depends on the initial configuration of the system.

In order to get a statistical distribution of the final misalignment we have integrated a series of 40 000

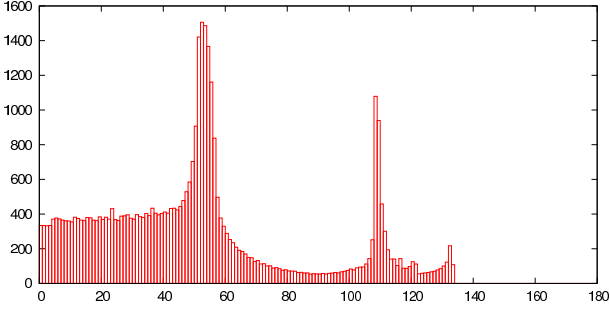


**Fig. 2** Histogram of the final distribution of the misalignment angle  $\theta_0$ . We have integrated a series of 40 000 systems with the same initial conditions from Table 1 except for the obliquity  $\theta_0 = 0^\circ$ , and inclination  $I$ , which range from  $\pm 84.3^\circ$  to  $90^\circ$ . We observe two pronounced peaks of higher probability around  $\theta_0 \approx 53^\circ$  and  $\theta_0 \approx 109^\circ$ , which is consistent with the observations of the Rossiter-McLaughlin anomaly for the HD 80606 system (Pont et al, 2009).

systems with the same initial conditions from Table 1 except for the obliquity of the star  $\theta_0 = 0^\circ$ , and for the mutual inclination  $I$ , which ranged from  $\pm 84.3^\circ$  to  $90^\circ$  (on an evenly spaced grid of  $-0.1 \leq \cos I \leq +0.1$ ). A histogram with the results of these simulations is given in Figure 2, with a bin width of  $1^\circ$ . Our results do not differ much from the histogram obtained by Fabrycky and Tremaine (2007), except that we observe two pronounced peaks of higher probability around  $\theta_0 \approx 53^\circ$  and  $\theta_0 \approx 109^\circ$ . They performed 1 000 simulations distributed in bins widths of  $10^\circ$ , which partially explains this difference, but the main reason is the fact that they adopted for the rotation of the star  $P_{\text{rot},0} = 10$  h, while we used a value closer to the Sun’s rotation period. Because we executed so much simulations our histogram is close to the probability density function distribution for the misalignment. Observations of the Rossiter-McLaughlin anomaly for the HD 80606 star reinforced the hypothesis of spin-orbit misalignment in this system (alignment excluded at  $> 95\%$  level), with a positive median projected angle of  $50^\circ$  (Pont et al, 2009). These observations are in perfect agreement with our simulations.

Although we used the full quadrupolar problem, while previous studies (Wu and Murray, 2003; Fabrycky and Tremaine, 2007) used the inner restricted problem (where the outer orbit is considered constant), we retrieve similar results and then verify that their approximation is appropriate for this specific situation.

#### 4.2 HD 98800

HD 98800 is an interesting and unusual system of four 10 Myr old post T-Tauri K stars: two spectroscopic binaries A and B in orbit about one another (Torres et al,

**Table 2** Initial parameters for the HD 98800 B system (Torres et al, 1995; Tokovinin, 1999).

HD 98800 B			
parameter	body 0	body 1	body 2
$m$ ( $M_\odot$ )	0.699	0.582	0.001
$P_{\text{rot}}$ (day)	20	0.5	—
$\theta$ (deg)	10	35	—
$\varphi$ (deg)	0	0	—
$R$ ( $\times 10^6$ m)	758	591	—
$C/mR^2$	0.08	0.08	—
$k_2$	0.028	0.028	—
$\Delta t$ (s)	100	100	—
parameter	orbit 1		orbit 2
$a$ (AU)	0.983		5.2
$e$	0.785		0.5
$\varpi$ (deg)	82.0		—
$I$ (deg)	20.0		

1995; Kastner et al, 1997). Moreover, it has a large infrared excess attributed to a circumbinary disc around the B pair (Koerner et al, 2000; Furlan et al, 2007). Substantial extinction towards this pair suggests that it is observed through some of this material (Tokovinin, 1999). An apparent absence of CO molecular gas in the disc combined with infrared spectrum modeling indicate that this is a T-Tauri transition disc that is just reaching the debris disc stage, with a collisional cascade having been recently initiated (e.g. Furlan et al, 2007). The orbits of the stars are all highly eccentric and inclined, creating a dynamical environment unlike almost all other known debris discs (Tokovinin, 1999). The dust disc is generally agreed to be an annulus around the B binary, but the exact structure varies from model to model. Koerner et al (2000) estimate a coplanar narrow ring outwards of about  $\sim 5$  AU from the two stars. However, Boden et al (2005) argue that the line of sight extinction means that the disc cannot be coplanar unless it is very flared.

Verrier and Evans (2009) investigated numerically the stability of a family of particles at large inclinations around the B binary, which remain stable even under the perturbation of an outer third stellar companion. The results show that the Lidov-Kozai mechanism of the outer star is disrupted by a nodal libration induced by the inner binary pair on a shorter time-scale. An analytical study by Farago and Laskar (2010) confirmed that equilibria at large inclination circumbinary orbits exist for the outer restricted quadrupolar problem. This raises the possibility that planets and asteroids with large inclination may survive in multi-stellar systems.

In this section we test the evolution of a Jupiter-like mass planet around the B binary in an orbit that is presently occupied by the dust disc. Since we average the orbit of the planet over the mean longitude, the

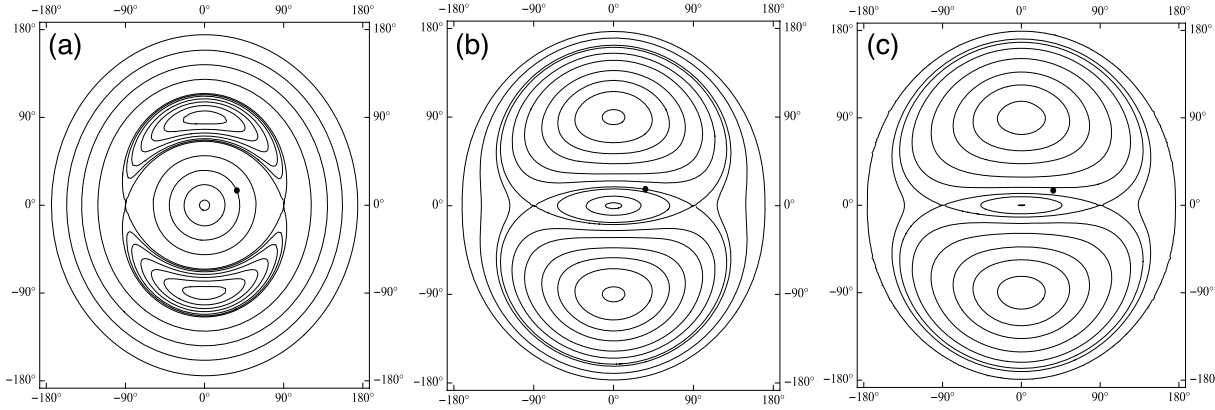


**Fig. 3** Energy levels in the  $(I \sin \varpi, I \cos \varpi)$  plane for different values of the eccentricity of the B binary HD 98800,  $e_1 = 0.5$  (a),  $e_1 = 0.785$  (b), and  $e_1 = 0.9$  (c) (Farago and Laskar, 2010). The dot marks the initial position of the outer orbit (Table 2).

orbital evolution of this planet can also be regarded as the orbital evolution of the particles in the disc. The HD 98800 system is still very young, and the B binary stars are very close to each other, so one can expect that the two components will undergo significant tidal evolution throughout its life. In order to speed-up the simulations we assume that both stars experience intense tidal dissipation, with  $\Delta t = 10^2$  s (Table 2). Because the gravitational effects of the A binary do not destabilize the system, we do not consider its presence in the simulations.

The inclination of the B binary with respect to the line of sight is estimated to be about  $23^\circ$  (Boden et al, 2005). The inclination of the disc with respect to the B binary is unknown, but one can contest its coplanarity, since substantial extinction of the light implies that the system is observed through some of this material (Tokovinin, 1999). Therefore, we assume that the inclination is about  $20^\circ$  (Table 2). The argument of the periaapsis and the longitude of the node were also determined with respect to the plane of the sky (Boden et al, 2005), but again, we miss the value of these two quantities measured with respect to the plane of the disc. As a consequence,  $\varpi_1$  is a free parameter for the planet/disc in our simulation. The choice of this parameter is critical, as it places the initial system in a different regime of libration, and it also determines the libration amplitude (Fig. 3b). Indeed, we can differentiate two kinds of regimes (Farago and Laskar, 2010): closed trajectories where the orbital angular momentum of the planet  $\mathbf{k}_2$  precesses around the orbital angular momentum of the binary  $\mathbf{k}_1$  (or its opposite  $-\mathbf{k}_1$ ); or closed trajectories where the orbital angular momentum of the planet precesses around the direction of the periaapsis of the binary  $\mathbf{e}_1$  (or its opposite  $-\mathbf{e}_1$ ). In the first situation the inclination is strictly inferior to  $90^\circ$  (or strictly superior to  $90^\circ$ , corresponding to a retro-

grade orbit), while in the second case the inclination oscillates around  $\pm 90^\circ$ .

In our simulation, we use  $\varpi_1 = 82^\circ$ , as this value places the initial orbit of the planet at the edge between the two different regimes of behavior (Fig. 3b). Initially,  $\mathbf{k}_2$  is precessing around  $\mathbf{k}_1$  and the mutual inclination oscillates between  $20^\circ$  and nearly  $90^\circ$ . As the system evolves, the norm of the orbital angular momentum of the planet remains constant, but the norm of the orbital angular momentum of the binary is modified by exchanges with the rotational angular momentum of the stars. Since we have considered  $\omega_1 \gg \omega_0$  (Table 2) in our example the initial exchanges are mainly between the binary's orbit and the spin of the star 1.

During the first stages of the evolution  $\omega_1 \gg n_1$  and the norm of the orbital angular momentum of the binary increases (Eq. 54), as well as the eccentricity and the semi-major axis (Eqs. 55, 56). As a consequence, the separatrix between the two regimes contracts (Fig. 3c). Since the norm of the orbital angular momentum of the planet remains constant (the planet is too far to undergo dissipation), the orbit of the planet crosses the separatrix and switches to the regime of precession around the direction of the periaapsis of the binary  $\mathbf{e}_1$ . In our simulation this transition occurs shortly after 80 Myr since we placed the initial system very close to the separatrix (Fig. 4a).

According to expression (51) the obliquity of the star  $\theta_1$  also increases, but the rotation rate decreases (Eq. 47). Around 2 Gyr, the obliquity begins to decrease and the orbit of the binary initiates its contraction. In general, this contraction is much slower than the previous expansion because the spin is already near an equilibrium position and the major source of dissipation becomes the orbital energy. As the eccentricity is damped, the separatrix between the two regimes expands and catches again the planet's orbit (Fig. 3b).

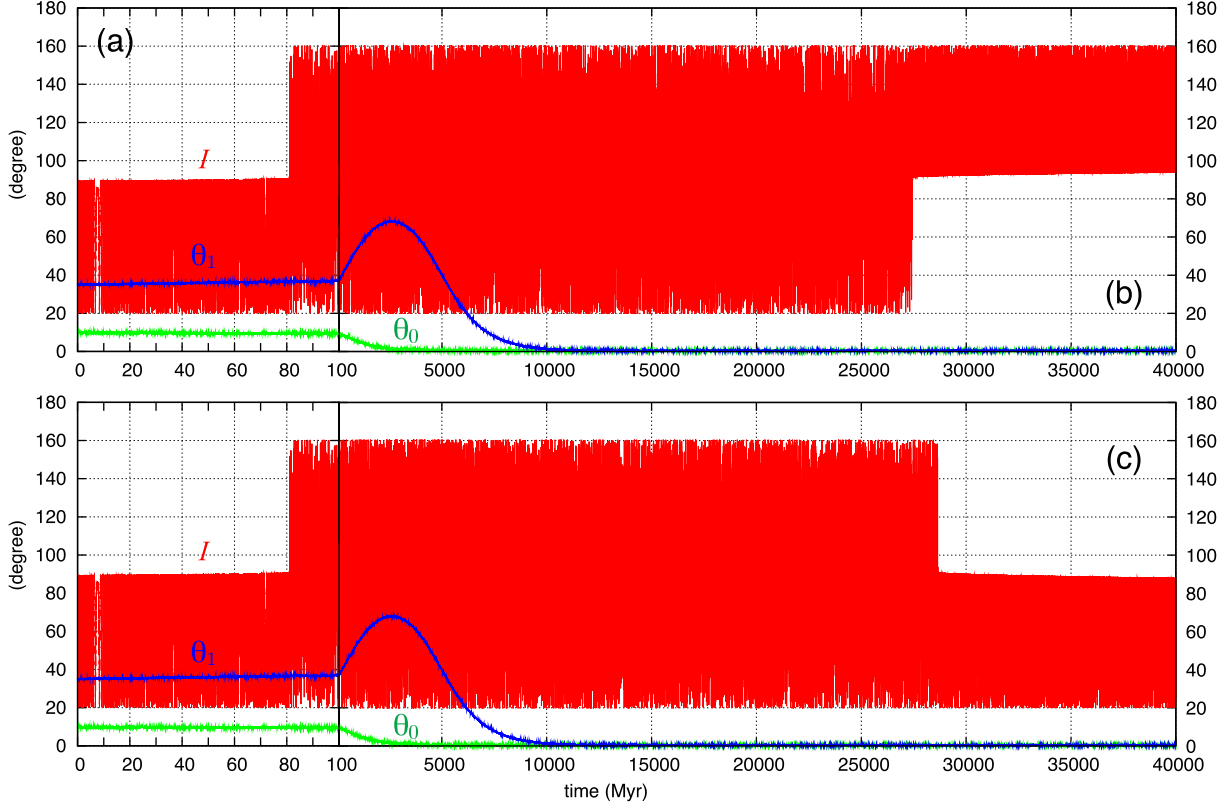


**Fig. 4** Possible evolutions for a  $m_2 \approx 10^{-3} M_\odot$  planet or disc at  $a_2 = 5.2$  AU and  $e_2 = 0.5$ , initially in a prograde orbit around the binary HD 98800 B (Table 2). During the first evolutionary stages the orbit of the binary expands and the planet changes of regime after about 80 Myr (a). As the binary orbit shrinks, the planet changes of regime again (somewhere between 25 and 30 Gyr), but depending when the planet crosses the separatrix between regimes, its orbit may become retrograde (b) or prograde (c).

After the second separatrix transition, the orbital angular momentum of the planet precesses again around the orbital angular momentum of the binary or its opposite  $\pm \mathbf{k}_1$ , depending on the  $\varpi_1$  value at the time the transition occurs. We have performed two different simulations, with a  $10^{-2}$  difference in the initial obliquity of the star  $\theta_0$ , and each one led to the a different final evolution scenario (Fig. 4b,c).

Subsequent tidal evolution of the binary orbit tends to circularize it. When the eccentricity reaches zero, the oscillations in the mutual inclination are also damped and the two angular momenta precess at constant inclination and speed (Fig. 3a). Tidal evolution in the inner binary is thus a very efficient mechanism of transforming initial prograde (or retrograde) orbits in retrograde (or prograde) orbits, although the norm of the angular momentum of the planet does not change.

#### 4.3 HD 11964

The planetary system around HD 11964 is composed of two planets with minimum masses  $m_1 = 25 M_\oplus$  (planet

c) and  $m_2 = 0.62 M_{\text{Jup}}$  (planet b), at  $a_1 = 0.229$  AU and  $a_2 = 3.16$  AU, respectively (Butler et al, 2006; Wright et al, 2009). Veras and Ford (2010) performed extensive n-body simulations for this system and concluded that it is always stable for mutual inclinations  $I < 60^\circ$  (or  $I > 120^\circ$ ), stable up to 85% for  $I < 75^\circ$  (or  $I > 105^\circ$ ), and stable up to 25% for  $75^\circ < I < 105^\circ$ . It is a system for which stability is possible for a wide range of mutual inclinations and thus perfect to apply our secular model.

Since the ratio between the semi-major axis of the two planets is  $a_2/a_1 \sim 14$ , the quadrupolar approximation is well suited, although octopole order terms in the development of the potential energy (Eq. 2) may cause variations and exchanges between the eccentricities of both planets. In order to test the quality of our secular model in the case of hierarchical planetary systems of this kind, we performed some direct n-body numerical simulations for the HD 11964 system and compared with the quadrupolar secular model. Results for the initial parameters in Table 3 are shown in Figure 5. We observe slightly additional variations in the amplitudes and precession rates of the eccentricity and inclination,

**Table 3** Initial parameters for the HD 11964 system (Butler et al, 2006; Wright et al, 2009).

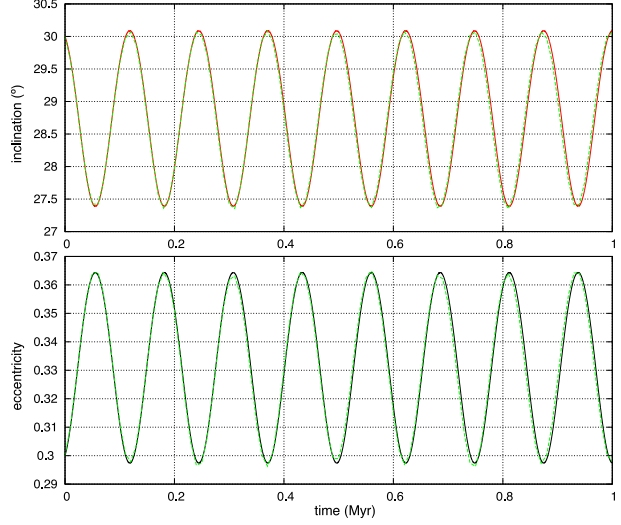
HD 11964			
parameter	body 0 ( <i>star</i> )	body 1 ( <i>c</i> )	body 2 ( <i>b</i> )
$m$ ( $M_{Jup}$ )	1178	0.0788	0.622
$P_{rot}$ (day)	20	0.5	—
$\theta$ (deg)	10	35	—
$\varphi$ (deg)	0	0	—
$R$ ( $\times 10^6 m$ )	695	75	—
$C/mR^2$	0.08	0.25	—
$k_2$	0.028	0.50	—
$\Delta t$ (s)	0.1	100	—
parameter	orbit 1 ( <i>c</i> )		orbit 2 ( <i>b</i> )
$a$ (AU)	0.229		3.16
$e$	0.300		0.041
$\varpi$ (deg)	0.0		—
$I$ (deg)	30.0		

but the general long-term behavior of the system remains essentially the same.

Though the present age of the star is estimated to be about 10 Gyr (Saffe et al, 2005), we start the system as if it has been recently formed. We assume the present orbits as the original ones, and an initial rotation period of the inner planet of about 10 h (Table 3). Because tidal effects on the inner planet are strong, the choice of the initial spin is irrelevant, as it evolves to an equilibrium configuration in about one million years (Figure 6a). Nevertheless, this procedure allows us to understand simultaneously the initial behavior of the system and also its future evolution. In addition, we arbitrarily assume a mutual inclination  $I = 30^\circ$ . This inclination value sets the system well outside a coplanar configuration, but yet below the critical value of about  $39^\circ$  that allows Lidov-Kozai cycles.

During the first million years (Figure 6a), the rotation rate of the inner planet and its obliquity are brought to their equilibrium positions, where one believe that the spin of the planet can be found today. The rotation rate is slowed down until it reaches an equilibrium near  $\omega_1/n_1 \approx f_2(e_1)/f_1(e_1)$ , that is,  $P_{rot,1} \approx 25$  d (Eq. 49), while the obliquity, after an initial increase (since the initial rotation rate is fast (Eq. 51)), quickly drops until it is captured in the small obliquity Cassini state  $\theta_1 \approx \sin I/\lambda_1 \approx 0.018^\circ$  (Eq. 53). Because the eccentricity and the inclination are oscillating, so does the equilibrium rotation rate (Eq. 48) and the equilibrium obliquity (Eq. 53).

During the first two million years (Figure 6a), the eccentricity and the inclination of the inner orbit do not experience any substantial secular modification (apart the periodical ones), since tidal effects are much less efficient over the orbit than over the spin. However, when

**Fig. 5** Evolution of the HD 11964 c inclination (top) and eccentricity (bottom) during 1 Myr, starting with the orbital solution from Wright et al (2009) and  $I = 30^\circ$  (Table 3). The solid lines curves are the values obtained with the quadrupolar secular model, while the dashed green lines are the complete solutions obtained with a n-body numerical model.

we follow the system over Gyr time-scales one can observe those variations occurring (Figure 6b). The most striking effect is an initial increase in the eccentricity of the inner planet, that is accompanied by a significant reduction in the mutual inclination between the orbits of the two planets. This behavior results from a combination of tidal effects, rotational flattening, and the gravitational perturbations from the outer planet, which tend to conserve the quantity  $h_1 = \sqrt{1 - e_1^2} \cos I$  (Eq. 45). Tidal effects alone also decrease the eccentricity (Eq. 55), so when its contribution becomes dominating the eccentricity is progressively damped to zero.

The exchanges between eccentricity and inclination (Fig. 5) are more significant for large values of the initial mutual inclination. The maximum value for the eccentricity oscillations is then higher and therefore the planet experiences stronger tidal effects. As a result, the orbit of the inner planet evolves in a shorter time-scale. In Figure 7 we plot the simultaneous evolution of the inclination and eccentricity of the inner orbit for different initial mutual inclinations,  $I$ . For  $I < 30^\circ$  there is almost no reduction in the inclination, and the eccentricity damping is very slow (Figure 7a). On the other hand, for  $I > 40^\circ$  we observe a reduction of more than  $20^\circ$  in the inclination, which is accompanied by an initial increase in the eccentricity, followed by a rapid damping to zero (Figure 7c,d).

For large values of the initial inclination, the system evolves much faster to its final configuration, so the orbit becomes circular in a shorter time-scale. Since the present orbit of the inner planet still presents an ec-

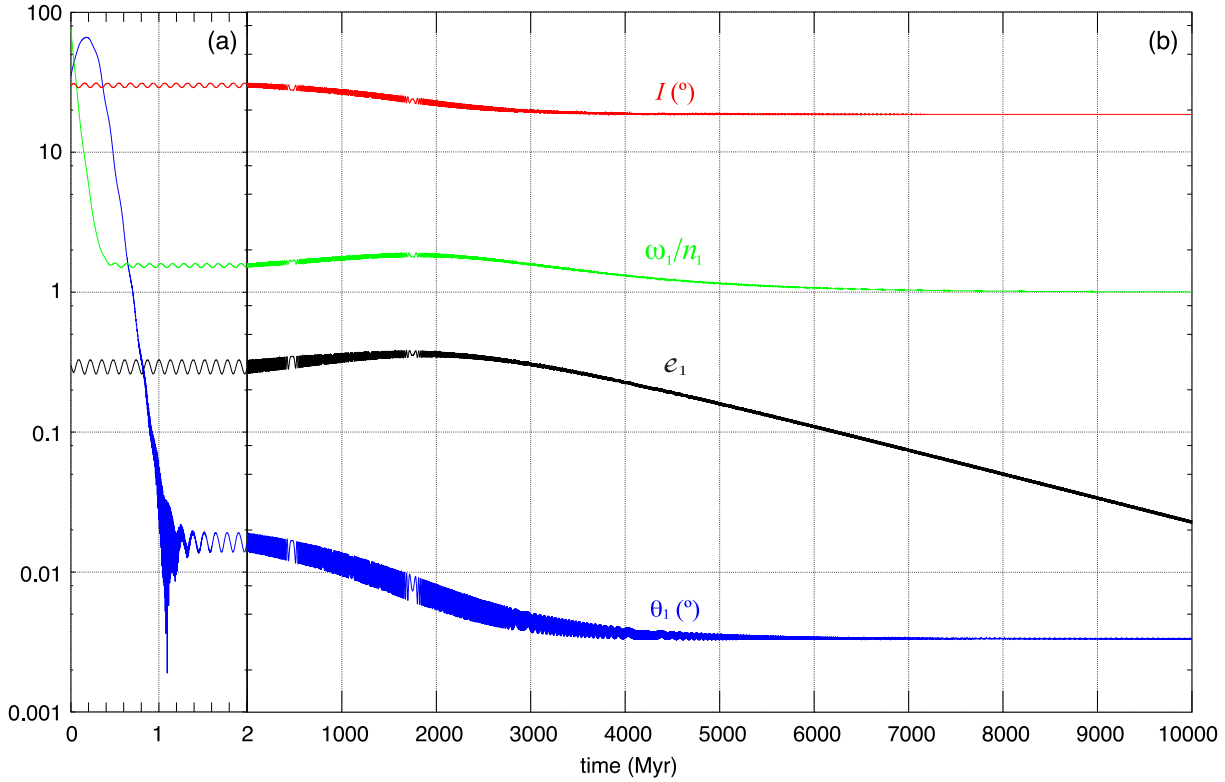


**Fig. 6** Long-term evolution of the planet HD 11964 c for an initial mutual inclination of  $30^\circ$  (Table 3). During the first million years, the rotation rate is slowed down into its equilibrium position (Eq. 48) and the obliquity is trapped in a small obliquity Cassini state (Eq. 53). As the system evolves, tidal effects decrease the mutual inclination of the planetary orbits, while the eccentricity increases until around 2 Gyr, time after which it is damped to zero. The rotation rate closely follows the eccentricity, and the obliquity also decreases, as the equilibrium in a Cassini state depends on the inclination of the perturber.

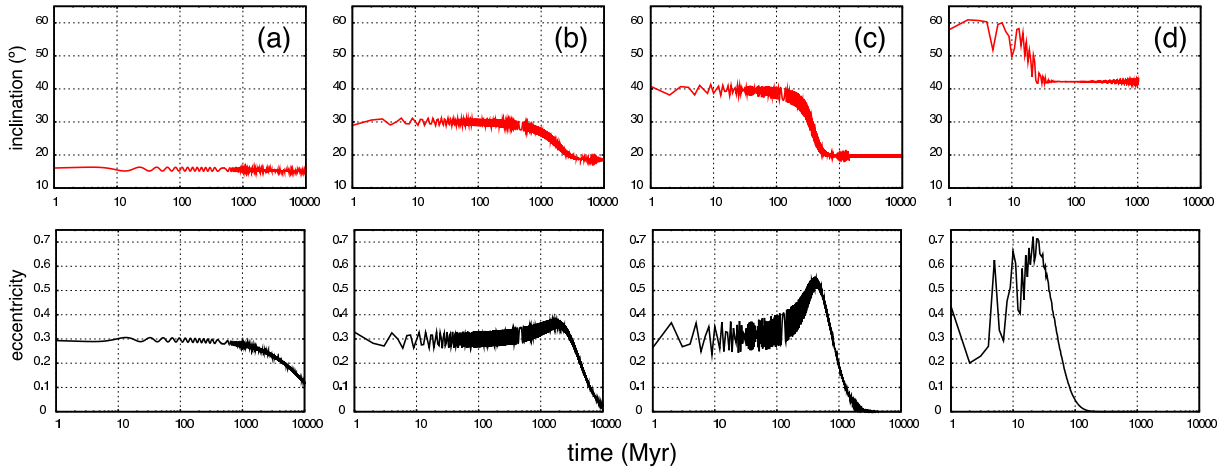


**Fig. 7** Long-term evolution of the inclination (top) and eccentricity (bottom) of the planet HD 11964 c for different values of the initial mutual inclination:  $15^\circ$  (a),  $30^\circ$  (b),  $40^\circ$  (c), and  $60^\circ$  (d) (Table 3). As the initial inclination increases, so does the amplitude of the eccentricity oscillations, resulting that tidal effects are enhanced, and the evolution time-scale shorter.



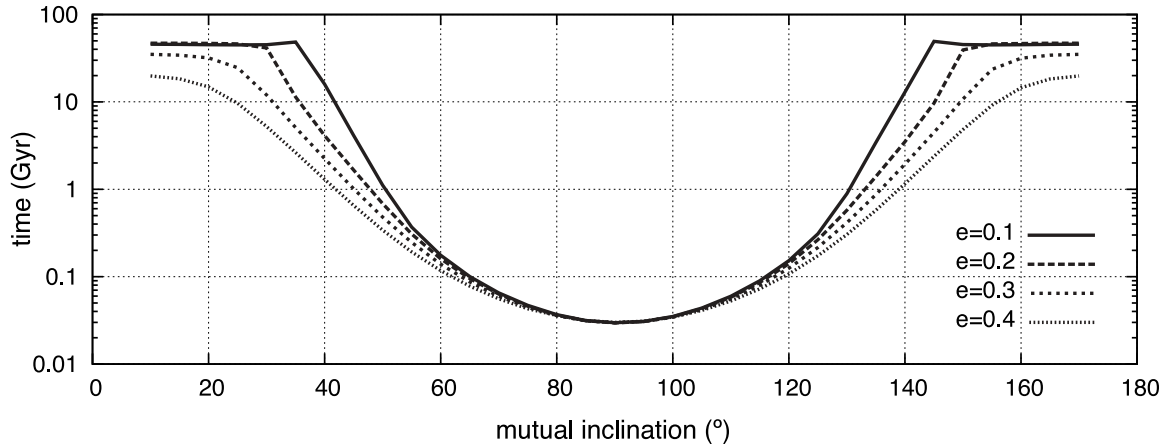


**Fig. 8** Time needed to circularize the orbit of the planet HD 11964 c ( $e_1 < 0.01$ ) as a function of the initial mutual inclination and for different values of the initial eccentricity ( $e_1 = 0.1, 0.2, 0.3$ , and  $0.4$ ). The system is 10 Gyr old (Saffe et al, 2005), so we conclude that initial inclinations between  $40^\circ$  and  $140^\circ$  were not possible, as the present eccentricity is still 0.3.

centricity close to 0.3, one may assume that the initial inclination could not have been excessively large. In order to estimate an upper limit for the initial inclination, we can run some simulations and check which of those can evolve to the present configuration within 10 Gyr, the estimated age for the system.

However, the choice of the initial orbit is not easy, since many different initial configurations can bring the planet to the present orbit, depending on the tidal damping coefficients ( $k_2$  and  $\Delta t$ ) and also on the initial eccentricity, inclination, and semi-major axis. It is out of the scope of this study to explore exhaustively the initial configurations of the HD 11964 system, but rather to illustrate some interesting evolutionary scenarios. As we just have seen, the present eccentricity combined with a large inclination can later evolve to an identical eccentricity but with smaller inclination. The semi-major axis will be slightly smaller than today, but this parameter essentially plays over the evolution time-scale. Thus, the present system can be a representation of the initial system and we adopt it for simplicity. In Figure 8 we used the initial conditions listed in Table 3, but modified the initial inclinations and eccentricities. We observe that inclinations in the interval  $[40^\circ, 140^\circ]$  circularize the orbit ( $e_1 < 0.01$ ) in less than 10 Gyr, so they can be discarded.

## 5 Conclusion

Many multi-planet systems have been reported in hierarchical configurations. For the most part, their mutual inclinations are unknown, but the fact that they exhibit significant values in the eccentricities led to think that the inclinations can also be large. In addition, very often the innermost planet in these systems is very close

to the star and undergoes tidal evolution. Here we have studied this particular sub-group of multi-planet systems. Using a very general and simplified averaged vectorial formalism, we have shown that inclined hierarchical planetary systems undergoing tidal dissipation can evolve in many different and sometimes unexpected ways.

We re-analyzed the case of HD 80606, a system where the planet migrated inwards by a combined tidal-Kozai mechanism, confirming previous results. We looked at the behavior of a planet (or disc) around the binary stars HD 98800 B and showed that initial prograde orbits may become retrograde and vice-versa, only because of tidal migration within the binary stars. Finally, we studied the regular 2-planet HD 11964 system and showed that tidal dissipation combined with gravitational perturbations may lead to a decrease in the mutual inclination, and a fast circularization of the inner orbit.

We have chosen the above three examples, as they are representative of the diversity of behaviors among inclined hierarchical systems. Many other systems are awaiting to be studied. The fact that we use average equations for both tidal and gravitational effects, makes our method suitable to be applied in long-term studies. It allows to run many simulations for different initial conditions in order to explore the entire phase space and evolutionary scenarios. In particular, it can be very useful to put constraints on the inclinations and dissipation ratios of hierarchical planetary systems. Our study can also be extended to systems of binary stars, and to planet-satellite systems.

**Acknowledgements** We acknowledge support from PNP-CNRS, France, and from Fundação para a Ciência e a Tecnologia, Portugal (grant PTDC/CTE-AST/098528/2008).

## A Averaged quantities

For completeness, we gather here the average formulae that are used in the computation of secular equations. Let  $F(\mathbf{r}, \dot{\mathbf{r}})$  be a function of a position vector  $\mathbf{r}$  and velocity  $\dot{\mathbf{r}}$ . Its averaged expression over the mean anomaly ( $M$ ) is given by

$$\langle F \rangle_M = \frac{1}{2\pi} \int_0^{2\pi} F(\mathbf{r}, \dot{\mathbf{r}}) dM. \quad (61)$$

Depending on the case, this integral is computed using the eccentric anomaly ( $E$ ), or the true anomaly ( $v$ ) as an intermediate variable. The basic formulae are

$$dM = \frac{r}{a} dE = \frac{r^2}{a^2 \sqrt{1-e^2}} dv,$$

$$\mathbf{r} = a(\cos E - e) \hat{\mathbf{e}} + a\sqrt{1-e^2}(\sin E) \hat{\mathbf{k}} \times \hat{\mathbf{e}},$$

$$\mathbf{r} = r \cos v \hat{\mathbf{e}} + r \sin v \hat{\mathbf{k}} \times \hat{\mathbf{e}},$$

$$\dot{\mathbf{r}} = \frac{na}{\sqrt{1-e^2}} \hat{\mathbf{k}} \times (\hat{\mathbf{r}} + \mathbf{e}),$$

$$r = a(1 - e \cos E) = \frac{a(1 - e^2)}{1 + e \cos v}, \quad (62)$$

where  $\hat{\mathbf{k}}$  is the unit vector of the orbital angular momentum, and  $\mathbf{e}$  the Laplace-Runge-Lenz vector (Eq. 3). We have then

$$\left\langle \frac{1}{r^3} \right\rangle = \frac{1}{a^3(1-e^2)^{3/2}}, \quad (63)$$

and

$$\left\langle \frac{\mathbf{r}^t \mathbf{r}}{r^5} \right\rangle = \frac{1}{2a^3(1-e^2)^{3/2}} (1 - \hat{\mathbf{k}}^t \hat{\mathbf{k}}), \quad (64)$$

which leads to

$$\left\langle \frac{1}{r^3} P_2(\hat{\mathbf{r}} \cdot \hat{\mathbf{u}}) \right\rangle = -\frac{1}{2a^3(1-e^2)^{3/2}} P_2(\hat{\mathbf{k}} \cdot \hat{\mathbf{u}}), \quad (65)$$

for any unit vector  $\hat{\mathbf{u}}$ . In the same way,

$$\langle r^2 \rangle = a^2 \left( 1 + \frac{3}{2} e^2 \right), \quad (66)$$

and

$$\langle \mathbf{r}^t \mathbf{r} \rangle = a^2 \frac{1-e^2}{2} (1 - \hat{\mathbf{k}}^t \hat{\mathbf{k}}) + \frac{5}{2} a^2 \mathbf{e}^t \mathbf{e}, \quad (67)$$

give

$$\langle r^2 P_2(\hat{\mathbf{r}} \cdot \hat{\mathbf{u}}) \rangle = -\frac{a^2}{2} \left( (1-e^2) P_2(\hat{\mathbf{k}} \cdot \hat{\mathbf{u}}) - 5e^2 P_2(\hat{\mathbf{e}} \cdot \hat{\mathbf{u}}) \right). \quad (68)$$

The other useful formulae are

$$\left\langle \frac{1}{r^6} \right\rangle = \frac{1}{a^6} f_1(e), \quad (69)$$

$$\left\langle \frac{1}{r^8} \right\rangle = \frac{1}{a^8 \sqrt{1-e^2}} f_2(e), \quad (70)$$

$$\left\langle \frac{\mathbf{r}^t \mathbf{r}}{r^8} \right\rangle = \frac{\sqrt{1-e^2}}{2a^6} f_4(e) (1 - \hat{\mathbf{k}}^t \hat{\mathbf{k}}) + \frac{6+e^2}{4a^6(1-e^2)^{9/2}} \mathbf{e}^t \mathbf{e}, \quad (71)$$

$$\left\langle \frac{\mathbf{r}}{r^8} \right\rangle = \frac{5}{2} \frac{1}{a^7 \sqrt{1-e^2}} f_4(e) \mathbf{e}, \quad (72)$$

$$\left\langle \frac{\mathbf{r}}{r^{10}} \right\rangle = \frac{7}{2} \frac{1}{a^9(1-e^2)} f_5(e) \mathbf{e}, \quad (73)$$

$$\left\langle \frac{(\mathbf{r} \cdot \dot{\mathbf{r}}) \mathbf{r}}{r^{10}} \right\rangle = \frac{n}{2a^7 \sqrt{1-e^2}} f_5(e) \hat{\mathbf{k}} \times \mathbf{e}, \quad (74)$$

where the  $f_i(e)$  functions are given by expressions (24) to (28).

Finally, for the average over the argument of the periapsis ( $\varpi$ ), we can proceed in an identical manner:

$$\langle \mathbf{e}^t \mathbf{e} \rangle_\varpi = \frac{1}{2\pi} \int_0^{2\pi} \mathbf{e}^t \mathbf{e} d\varpi = \frac{e^2}{2} (1 - \mathbf{k}^t \mathbf{k}), \quad (75)$$

which gives

$$\langle (\mathbf{e} \cdot \hat{\mathbf{u}}) \mathbf{e} \rangle_\varpi = \frac{e^2}{2} (\hat{\mathbf{u}} - (\mathbf{k} \cdot \hat{\mathbf{u}}) \mathbf{k}). \quad (76)$$

## References

- Boden AF, Sargent AI, Akeson RL, Carpenter JM, Torres G, Latham DW, Soderblom DR, Nelan E, Franz OG, Wasserman LH (2005) Dynamical Masses for Low-Mass Pre-Main-Sequence Stars: A Preliminary Physical Orbit for HD 98800 B. *Astrophys. J.* 635:442–451, DOI 10.1086/497328, arXiv:astro-ph/0508331
- Boué G, Laskar J (2006) Precession of a planet with a satellite. *Icarus* 185:312–330, DOI 10.1016/j.icarus.2006.07.019
- Boué G, Laskar J (2009) Spin axis evolution of two interacting bodies. *Icarus* 201:750–767, DOI 10.1016/j.icarus.2009.02.001
- Butler RP, Wright JT, Marcy GW, Fischer DA, Vogt SS, Tinney CG, Jones HRA, Carter BD, Johnson JA, McCarthy C, Penny AJ (2006) Catalog of Nearby Exoplanets. *Astrophys. J.* 646:505–522, DOI 10.1086/504701, arXiv:astro-ph/0607493
- Chatterjee S, Ford EB, Matsumura S, Rasio FA (2008) Dynamical Outcomes of Planet-Planet Scattering. *Astrophys. J.* 686:580–602, DOI 10.1086/590227, arXiv:astro-ph/0703166
- Colombo G (1966) Cassini's second and third laws. *Astron. J.* 71:891–896
- Correia ACM (2009) Secular Evolution of a Satellite by Tidal Effect: Application to Triton. *Astrophys. J.* 704:L1–L4, DOI 10.1088/0004-637X/704/1/L1, 0909.4210
- Correia ACM, Laskar J (2004) Mercury's capture into the 3/2 spin-orbit resonance as a result of its chaotic dynamics. *Nature* 429:848–850, DOI 10.1038/nature02609
- Correia ACM, Laskar J (2009) Mercury's capture into the 3/2 spin-orbit resonance including the effect of core-mantle friction. *Icarus* 201:1–11, DOI 10.1016/j.icarus.2008.12.034, 0901.1843
- Correia ACM, Laskar J (2010a) Long-term evolution of the spin of Mercury. I. Effect of the obliquity and core-mantle friction. *Icarus* 205:338–355, DOI 10.1016/j.icarus.2009.08.006, 0908.3912
- Correia ACM, Laskar J (2010b) Tidal Evolution of Exoplanets. In: *Exoplanets*, University of Arizona Press, pp 534–575
- Correia ACM, Laskar J, Néron de Surgy O (2003) Long-term evolution of the spin of Venus I. Theory. *Icarus* 163:1–23, DOI 10.1016/S0019-1035(03)00042-3
- D'Angelo C, van Kerkwijk MH, Rucinski SM (2006) Contact Binaries with Additional Components. II. A Spectroscopic Search for Faint Tertiaries. *Astron. J.* 132:650–662, DOI 10.1086/505265, arXiv:astro-ph/0602139



- Efroimsky M, Williams JG (2009) Tidal torques: a critical review of some techniques. *Celestial Mechanics and Dynamical Astronomy* 104:257–289, DOI 10.1007/s10569-009-9204-7, 0803.3299
- Eggenberger A, Udry S, Mayor M (2004) Statistical properties of exoplanets. III. Planet properties and stellar multiplicity. *Astron. Astrophys.* 417:353–360, DOI 10.1051/0004-6361:20034164, arXiv:astro-ph/0402664
- Eggleton PP, Kiseleva-Eggleton L (2001) Orbital Evolution in Binary and Triple Stars, with an Application to SS Lacertae. *Astrophys. J.* 562:1012–1030, DOI 10.1086/323843, arXiv:astro-ph/0104126
- Fabrycky D, Tremaine S (2007) Shrinking Binary and Planetary Orbits by Kozai Cycles with Tidal Friction. *Astrophys. J.* 669:1298–1315, DOI 10.1086/521702, 0705.4285
- Farago F, Laskar J (2010) High-inclination orbits in the secular quadrupolar three-body problem. *Mon. Not. R. Astron. Soc.* 401:1189–1198, DOI 10.1111/j.1365-2966.2009.15711.x, 0909.2287
- Fischer DA, Marcy GW, Butler RP, Vogt SS, Frink S, Apps K (2001) Planetary Companions to HD 12661, HD 92788, and HD 38529 and Variations in Keplerian Residuals of Extrasolar Planets. *Astrophys. J.* 551:1107–1118, DOI 10.1086/320224
- Ford EB, Kozinsky B, Rasio FA (2000) Secular Evolution of Hierarchical Triple Star Systems. *Astrophys. J.* 535:385–401, DOI 10.1086/308815
- Furlan E, Sargent B, Calvet N, Forrest WJ, D’Alessio P, Hartmann L, Watson DM, Green JD, Najita J, Chen CH (2007) HD 98800: A 10 Myr Old Transition Disk. *Astrophys. J.* 664:1176–1184, DOI 10.1086/519301, 0705.0380
- Kastner JH, Zuckerman B, Weintraub DA, Forveille T (1997) X-ray and molecular emission from the nearest region of recent star formation. *Science* 277:67–71, DOI 10.1126/science.277.5322.67
- Kaula WM (1964) Tidal dissipation by solid friction and the resulting orbital evolution. *Rev. Geophys.* 2:661–685
- Koerner DW, Jensen ELN, Cruz KL, Guild TB, Gultekin K (2000) A Single Circumbinary Disk in the HD 98800 Quadruple System. *Astrophys. J.* 533:L37–L40, DOI 10.1086/312593, arXiv:astro-ph/0002227
- Kozai Y (1962) Secular perturbations of asteroids with high inclination and eccentricity. *Astron. J.* 67:591–598, DOI 10.1086/108790
- Lambeck K (1988) *Geophysical geodesy : the slow deformations of the earth* Lambeck. Oxford [England] : Clarendon Press ; New York : Oxford University Press, 1988.
- Laskar J (1997) Large scale chaos and the spacing of the inner planets. *Astron. Astrophys.* 317:L75–L78
- Laskar J, Boué G (2010) Explicit expansion of the three-body disturbing function for arbitrary eccentricities and inclinations. *Astron. Astrophys.* 522:A60+, DOI 10.1051/0004-6361/201014496, 1008.2947
- Lee MH, Peale SJ (2003) Secular Evolution of Hierarchical Planetary Systems. *Astrophys. J.* 592:1201–1216, DOI 10.1086/375857, arXiv:astro-ph/0304454
- Lidov ML (1961) Evolution of the planets artificial satellites orbits under effect of the outer bodies gravity perturbations. *Iskus sputniky Zemly (in Russian)* 8:5–45
- Lidov ML (1962) The evolution of orbits of artificial satellites of planets under the action of gravitational perturbations of external bodies. *Plan. Space Sci.* 9:719–759, DOI 10.1016/0032-0633(62)90129-0
- Lidov ML, Ziglin SL (1976) Non-restricted double-averaged three body problem in Hill’s case. *Celestial Mechanics* 13:471–489, DOI 10.1007/BF01229100
- Marchal C (1990) *The Three-Body Problem*. Elsevier, Amsterdam
- Migaszewski C, Goździewski K (2009) Secular dynamics of a coplanar, non-resonant planetary system under the general relativity and quadrupole moment perturbations. *Mon. Not. R. Astron. Soc.* 392:2–18, DOI 10.1111/j.1365-2966.2008.14025.x, 0809.5248
- Mignard F (1979) The evolution of the lunar orbit revisited. *I. Moon and Planets* 20:301–315
- Naef D, Latham DW, Mayor M, Mazeh T, Beuzit JL, Drukier GA, Perrier-Bellet C, Queloz D, Sivan JP, Torres G, Udry S, Zucker S (2001) HD 80606 b, a planet on an extremely elongated orbit. *Astron. Astrophys.* 375:L27–L30, DOI 10.1051/0004-6361:20010853, arXiv:astro-ph/0106256
- Nagasawa M, Ida S, Bessho T (2008) Formation of Hot Planets by a Combination of Planet Scattering, Tidal Circularization, and the Kozai Mechanism. *Astrophys. J.* 678:498–508, DOI 10.1086/529369, 0801.1368
- Néron de Surgy O, Laskar J (1997) On the long term evolution of the spin of the Earth. *Astron. Astrophys.* 318:975–989
- Palacián JF, Yanguas P, Fernández S, Nicotra MA (2006) Searching for periodic orbits of the spatial elliptic restricted three-body problem by double averaging. *Physica D Nonlinear Phenomena* 213:15–24, DOI 10.1016/j.physd.2005.10.009
- Peale SJ (1969) Generalized Cassini’s Laws. *Astron. J.* 74:483–489
- Pont F, Hébrard G, Irwin JM, Bouchy F, Moutou C, Ehrenreich D, Guillot T, Aigrain S, Bonfils X, Berta Z, Boisse I, Burke C, Charbonneau D, Delfosse X, Desort M, Eggenberger A, Forveille T, Lagrange A, Lovis C, Nutzman P, Pepe F, Perrier C, Queloz D, Santos NC, Ségransan D, Udry S, Vidal-Madjar A (2009) Spin-orbit misalignment in the HD 80606 planetary system. *Astron. Astrophys.* 502:695–703, DOI 10.1051/0004-6361/200912463, 0906.5605
- Pont F, Husnoo N, Mazeh T, Fabrycky D (2011) Determining eccentricities of transiting planets: a divide in the mass-period plane. *Mon. Not. R. Astron. Soc.* pp 378–+, DOI 10.1111/j.1365-2966.2011.18462.x, 1103.2081
- Saffe C, Gómez M, Chavero C (2005) On the ages of exoplanet host stars. *Astron. Astrophys.* 443:609–626, DOI 10.1051/0004-6361:20053452, arXiv:astro-ph/0510092
- Schutz BF (1985) *A First Course in General Relativity*. Cambridge University Press
- Singer SF (1968) The Origin of the Moon and Geophysical Consequences. *Geophys. J. R. Astron. Soc.* 15:205–226
- Smart WM (1953) *Celestial Mechanics*. London, New York, Longmans, Green
- Tokovinin A, Thomas S, Sterzik M, Udry S (2006) Tertiary companions to close spectroscopic binaries. *Astron. Astrophys.* 450:681–693, DOI 10.1051/0004-6361:20054427, arXiv:astro-ph/0601518
- Tokovinin AA (1999) The visual orbit of HD 98800. *Astronomy Letters* 25:669–671
- Torres G, Stefanik RP, Latham DW, Mazeh T (1995) Study of Spectroscopic Binaries with TODCOR. IV. The Multiplicity of the Young Nearby Star HD 98800. *Astrophys. J.* 452:870–+, DOI 10.1086/176355
- Tremaine S, Touma J, Namouni F (2009) Satellite Dynamics on the Laplace Surface. *Astron. J.* 137:3706–3717, DOI 10.1088/0004-6256/137/3/3706, 0809.0237
- TriAUD AHMJ, Collier Cameron A, Queloz D, Anderson DR, Gillon M, Hebb L, Hellier C, Loeillet B, Maxted PFL, Mayor M, Pepe F, Pollacco D, Ségransan D, Smalley B, Udry S, West RG, Wheatley PJ (2010) Spin-orbit angle

- measurements for six southern transiting planets. New insights into the dynamical origins of hot Jupiters. *Astron. Astrophys.* 524:A25+, DOI 10.1051/0004-6361/201014525, 1008.2353
- Veras D, Ford EB (2010) Secular Orbital Dynamics of Hierarchical Two-planet Systems. *Astrophys. J.* 715:803–822, DOI 10.1088/0004-637X/715/2/803, 1004.1421
- Verrier PE, Evans NW (2009) High-inclination planets and asteroids in multistellar systems. *Mon. Not. R. Astron. Soc.* 394:1721–1726, DOI 10.1111/j.1365-2966.2009.14446.x, 0812.4528
- Ward WR, Hamilton DP (2004) Tilting Saturn. I. Analytic Model. *Astron. J.* 128:2501–2509, DOI 10.1086/424533
- Wright JT, Upadhyay S, Marcy GW, Fischer DA, Ford EB, Johnson JA (2009) Ten New and Updated Multiplanet Systems and a Survey of Exoplanetary Systems. *Astrophys. J.* 693:1084–1099, DOI 10.1088/0004-637X/693/2/1084, 0812.1582
- Wu Y, Goldreich P (2002) Tidal Evolution of the Planetary System around HD 83443. *Astrophys. J.* 564:1024–1027, DOI 10.1086/324193, arXiv:astro-ph/0108499
- Wu Y, Murray N (2003) Planet Migration and Binary Companions: The Case of HD 80606b. *Astrophys. J.* 589:605–614, DOI 10.1086/374598, arXiv:astro-ph/0303010